Mineralogy and Petrology (2018) 112:647–670
https://doi.org/10.1007/s00710-018-0559-x

ORIGINAL PAPER

Fluid circulations in response to mantle exhumation at the passive margin setting in the north Pyrenean zone, France

B. Corre[1] · P. Boulvais[1] · M. C. Boiron[2] · Y. Lagabrielle[1] · L. Marasi[1] · C. Clerc[3]

Received: 14 June 2017 / Accepted: 19 February 2018 / Published online: 28 February 2018

Abstract

Sub-continental lithospheric mantle rocks are exhumed in the distal part of magma-poor passive margins. Remnants of the North Iberian paleo-passive margin are now exposed in the North–Pyrenean Zone (NPZ) and offers a field analogue to study the processes of continental crust thinning, subcontinental mantle exhumation and associated fluid circulations. The Saraillé Massif which belongs to the 'Chaînons Béarnais' range (Western Pyrenees), displays field, petrographic and stable isotopic evidence of syn-kinematic fluid circulations. Using electron probe micro-analyses on minerals, O, C, Sr isotopes compositions and micro thermometry/Raman spectrometry of fluid inclusions, we investigate the history of fluid circulations along and in the surroundings of the Saraillé detachment fault. The tectonic interface between the pre-rift Mesozoic sedimentary cover and the mantle rocks is marked by a metasomatic talc-chlorite layer. This layer formed through the infiltration of a fluid enriched in chemical elements like Cr leached from the exhuming serpentinized mantle rocks. In the overlying sediments (dolomitic and calcitic marbles of Jurassic to Aptian age), a network of calcitic veins, locally with quartz, formed as a consequence of the infiltration of aqueous saline fluids (salinities up to 34 wt% NaCl are recorded in quartz-hosted fluid inclusions) at moderate temperatures (~ 220 °C). These brines likely derived from the dissolution of the local Triassic evaporites. In the upper part of the metasomatic system, upward movement of fluids is limited by the Albian metasediments, which likely acted as an impermeable layer. The model of fluid circulation in the Saraillé Massif sheds light onto other synchronous metasomatic systems in the Pyrenean realm.

Keywords Mantle exhumation · Passive margins · Fluid circulations · Fluid inclusions · Stable isotopes · North-Pyrenean Zone

Introduction

Sub-continental lithospheric mantle rocks are exhumed at the foot of magma-poor distal passive margins as a response to extreme stretching of the continental crust during plate separation. The processes of fluid-rock interactions during such a major step of the plate tectonics cycle led to metal deposition, impact the reservoir properties of pre- and syn-rift sediments, may influence the chemistry of seawater (e.g. Pinto et al. 2015). They have been often considered in the exhumed mantle lithosphere but are still poorly investigated in a complete system associating both the exhumed ultramafic rocks and the extremely thinned continental basement (e.g. Roberston 2007; Pinto et al. 2015; Incerpi et al. 2017). The most complete studies were first conducted thanks to drilling through Ocean Continent Transition (OCT) such as the Iberia-Newfoundland margins (Péron-Pinvidic and Manatschal 2009) and recent back-arc basins such as the Tyrrhenian sea (Bonatti et al. 1990). However, in these examples, the continental basement remnants are rare and only few vertical cores have been drilled through hyper-thinned crustal units. Thus, the horizontal and vertical continuity of fluid migrations cannot be fully evaluated in the present-day passive margins systems.

Editorial handling: M. A.T.M. Broekmans

✉ B. Corre
benjamin.corre@univ-rennes1.fr

[1] Univ Rennes, CNRS, Géosciences Rennes, UMR 6118, F-35000 Rennes, France

[2] GeoRessources, UMR, Université de Lorraine – CNRS – CREGU, Boulevard des Aiguillettes, BP 70239, F-54506 Vandoeuvre-lès-Nancy, France

[3] Institut des Sciences Exactes et Appliquées (ISEA), University of New Caledonia, Av. James Cook, BP R4, 98800 Nouméa, France

An alternative strategy is to focus on paleo-passive margin remnants now exposed in orogenic belts where three-dimensional in situ observations are possible (Manatschal 2004; Lagabrielle and Bodinier 2008; Péron-Pinvidic and Manatschal 2009). Important information was obtained recently by investigating the onland analogues of the Alpine paleomargin (Manatschal and Nievergelt 1997; Manatschal and Müntener 2009; Pinto et al. 2015; Incerpi et al. 2017). Also the Pyrenean belt in the North Pyrenean Zone (NPZ) well preserved remnants of inverted distal passive margins including bodies of exhumed mantle (Lagabrielle and Bodinier 2008; Jammes et al. 2009; Lagabrielle et al. 2010). It has been shown that a significant amount of fluids have circulated at a regional scale during the extension of the continental crust of the NPZ during Cretaceous times (e.g. Dauteuil and Ricou 1989). Major effects are the albitization of the plutonic basement (Boulvais et al. 2007; Poujol et al. 2010; Fallourd et al. 2014) and the formation of metasomatic rocks such as talc-chlorite deposits (Moine et al. 1989; Schärer et al. 1999; Boulvais et al. 2006; Boiron et al. 2007; Boutin et al. 2015). In addition, some portions of the western NPZ allow a 3D reconstruction of the very distal portion of the passive margin including its three classical components:

(1) serpentinized subcontinental peridotites,
(2) extremely thinned continental basement rocks and
(3) remnants of pre-rift sedimentary cover (Corre et al. 2016).

Taken together, these arguments strongly imply that the NPZ might present an excellent example to study the role of fluid-rock interactions during mantle exhumation (Salardon et al. 2017).

The Saraillé massif in the Chaînons Béarnais (western NPZ) exhibits marks of intense fluid migration related to mantle exhumation that occurred in the pre-orogenic times (Corre et al. 2016; Salardon et al. 2017). In their detailed mapping of the Saraillé massif, Fortané et al. (1986) described a foliated talc-rich layer located between the lherzolites and the Mesozoic sediments. They evidenced the presence of talc, clinochlore and pyrite, an association representative of greenschist facies conditions (250–350 °C). In this paper, we describe the abundant veining observed in both tectonic lenses of crustal basement and ductilely deformed metasediments to highlight fluid-assisted deformation in the Saraillé metasomatic system. We also present the characteristics of fluid inclusions in vein minerals and the oxygen, carbon and strontium isotope compositions of veins and of their host rocks. An internally consistent model of fluid circulation is proposed. We finally discuss the implications of our results at the scale of the Pyrenees.

Geological setting

The Pyrenean belt and the NPZ

The Pyrenees is an E-W trending belt corresponding to a shortened crustal domain that spread between the Iberia and Europe plates during Cretaceous times (Choukroune 1992). The pre-Pyrenean (Cretaceous) extensional phase resulted from the rotational movement of the Iberia plate relative to the Europe plate in relation with the opening of the Central Atlantic and the Bay of Biscay (Choukroune and Mattauer 1978; Olivet 1996; Sibuet et al. 2004; Gong et al. 2009). This phase is characterized by an extreme thinning of the continental crust leading to the local exhumation of subcontinental mantle rocks to the floor of Albian-Cenomanian basins. The tectonic inversion of these Albian-Cenomanian basins starting in the Late Cretaceous times resulted in the stacking of units forming the present-day NPZ (Choukroune 1989; Muñoz 1992; Vacherat et al. 2016) (NPZ; Fig. 1).

The E-W trending NPZ is limited to the north by the North Pyrenean Frontal Thrust (NPFT) and to the south by the North Pyrenean Fault (NPF) (Fig. 1). This structural domain is constituted of folded and faulted pre-rift and syn-rift sedimentary cover of Mesozoic age associated with about 40 bodies of sub-continental peridotites and remnants of a stretched continental basement exposed in the North-Pyrenean massifs. The NPZ is also characterized by a high-temperature low-pressure (HT-LP) metamorphism, well recorded in metasediments, which developed in relation with the mid-Cretaceous extensional event (Golberg and Leyreloup 1990; Clerc et al. 2015) (Fig. 1).

The Saraillé massif

The Saraillé massif is located in the Chaînons Béarnais, a group of three E-W trending thrust-folds in the western part of the NPZ. It is exposed on the southern border of the central Sarrance anticline (Fig. 2a, b; see also Corre et al. 2016). Detailed mapping of the Saraillé massif has shown that the overall structure corresponds to a south-verging recumbent thrust fold of the pre-rift Mesozoic metasedimentary cover wrapping several thin lenses of Paleozoic basement welded on core of serpentinized lherzolite (Fig. 3a, b, c). The tectonic interface between the metasediments and the mantle rocks is characterized by a 20 m thick talc-chlorite schist layer. Corre et al. (2016) have shown that this layer is a remnant of the shallower section of the detachment zone along which mantle rocks were exhumed during the formation of the North Iberia passive margin. They also demonstrated that during its extreme attenuation, the continental basement was reduced to tectonic lenses some tens of meters thick by ductile shearing and that the Mesozoic pre-rift sediments

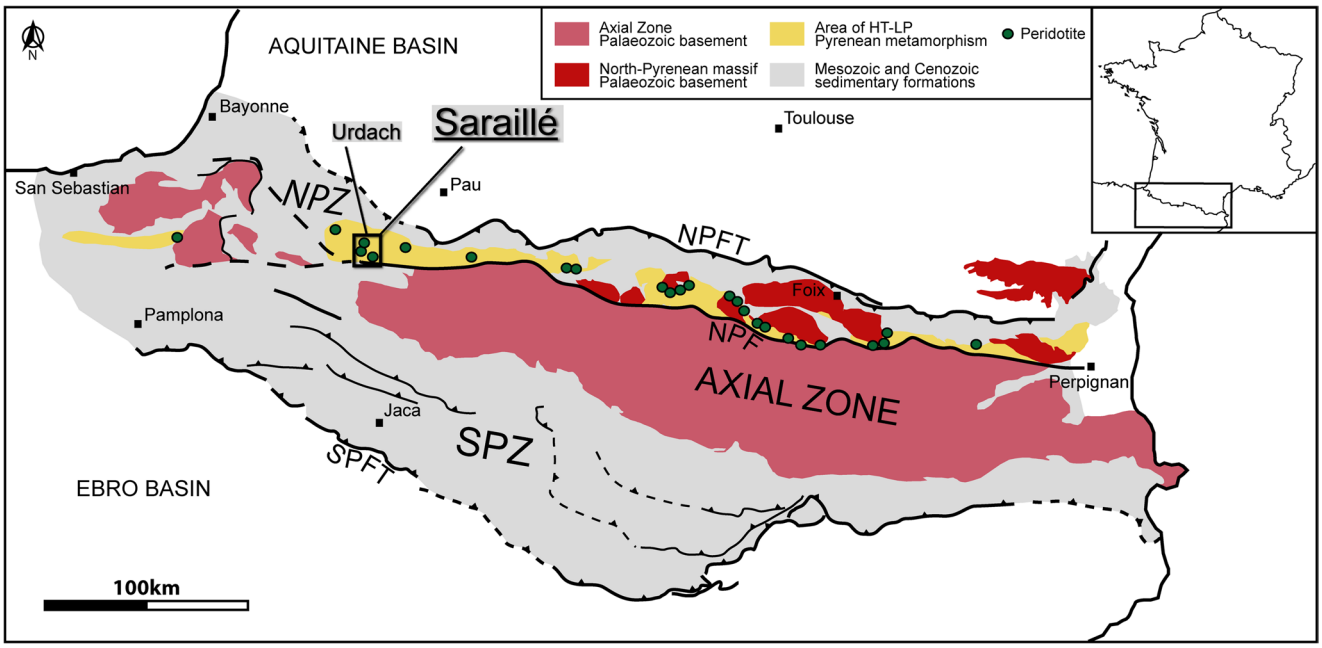

Fig. 1 Structural map of the Pyrenees with indication of the studied zone in the 'Chaînons Béarnais'. NPFT: North-Pyrenean Frontal Thrust, NPF: North-Pyrenean Fault, SPFT: South Pyrenean Frontal Thrust (after Clerc and Lagabrielle 2014; Vauchez et al. 2013)

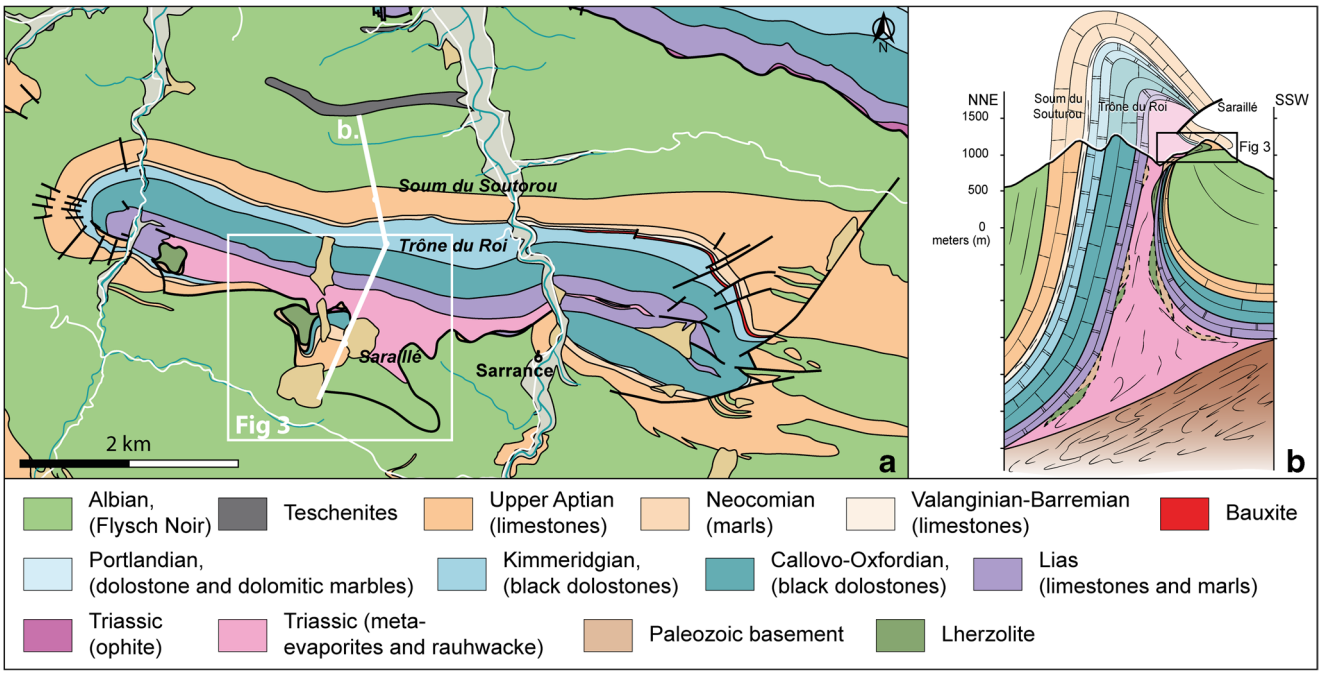

Fig. 2 **a** Geological map of the Sarrance anticline with indication of the cross section. **b** Geological cross-section of the Sarrance anticline crossing the Saraillé massif

experienced syn-metamorphic ductile thinning (Fig. 4). As a result, a well defined S0/S1 foliation is locally observed in the ductilely flattened marbles.

The Mesozoic sequence consists of Triassic to Albian metasediments which experienced boudinage during the Cretaceous extension (Corre et al. 2016) (Fig. 4). Thinning is maximum at the place where mantle rocks have been exhumed. The Triassic metasediments, exposed in the core of the Sarrance anticline, include motley calc schists, rhaunwacke (cellular dolomite), brecciated dolomitic marbles and

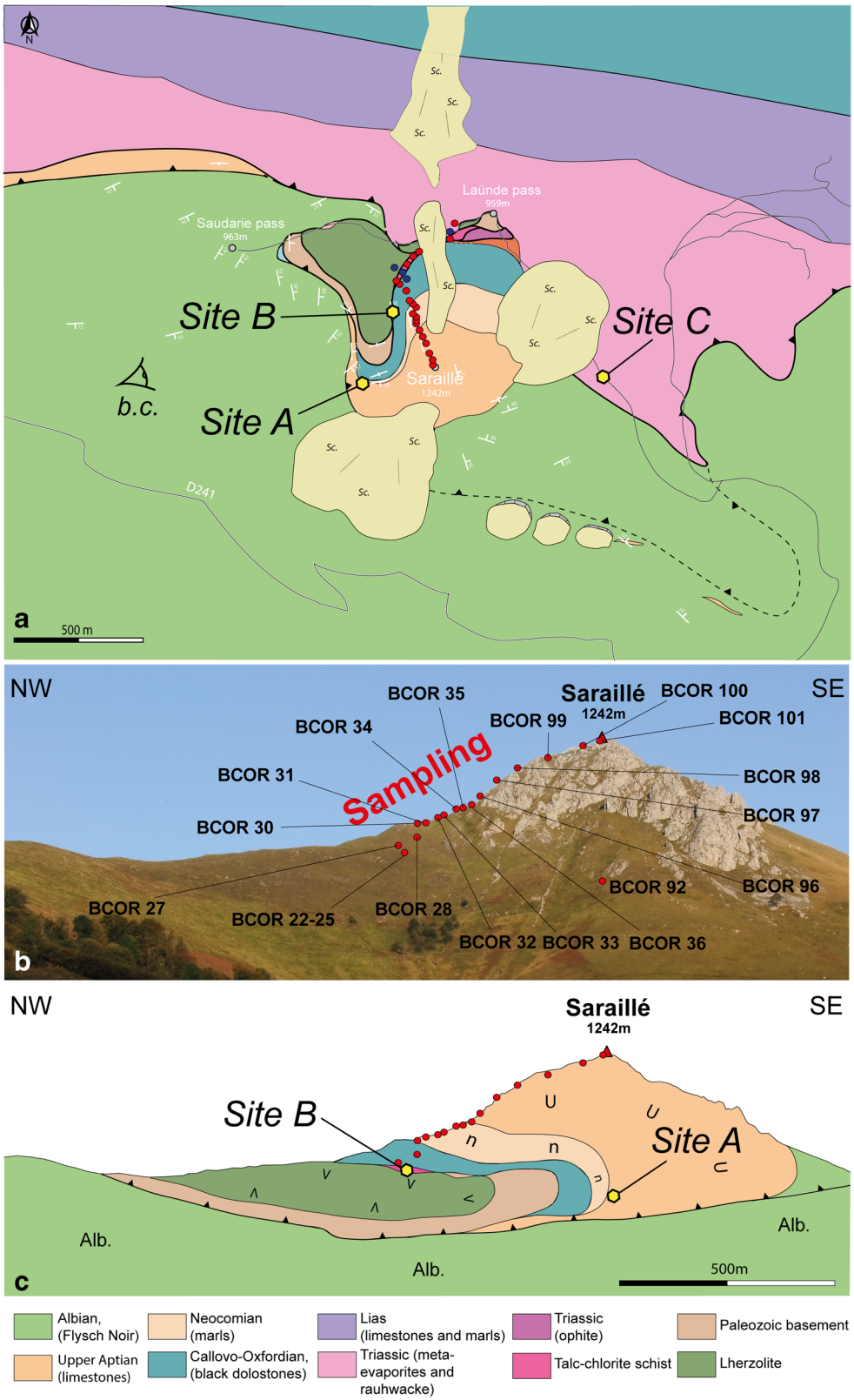

Fig. 3 **a** Detailed geological map of the Saraillé massif with samples locations (red: samples for stable isotopes and fluid inclusions (BCOR); blue: samples for Electron microprobe analyses (SAR), see Fig. 2 for location. **b** Panorama view of the Saraillé massif with samples locations. **c** Interpreted geological panorama view of the Saraillé massif. n: Neocomian, U: Urgonian (Upper Aptian). See Fig. 2 for the legend

meta-ophites, often with a cataclastic fabric. The Jurassic sequence is represented by variably deformed dolomitic marbles. The Neocomian sequence comprises dolomitic marbles, pure calcitic marbles and phyllite-rich marbles. The Upper Aptian sequence consists of metamorphosed Urgonian facies platform carbonates, characterized by numerous rudists, often

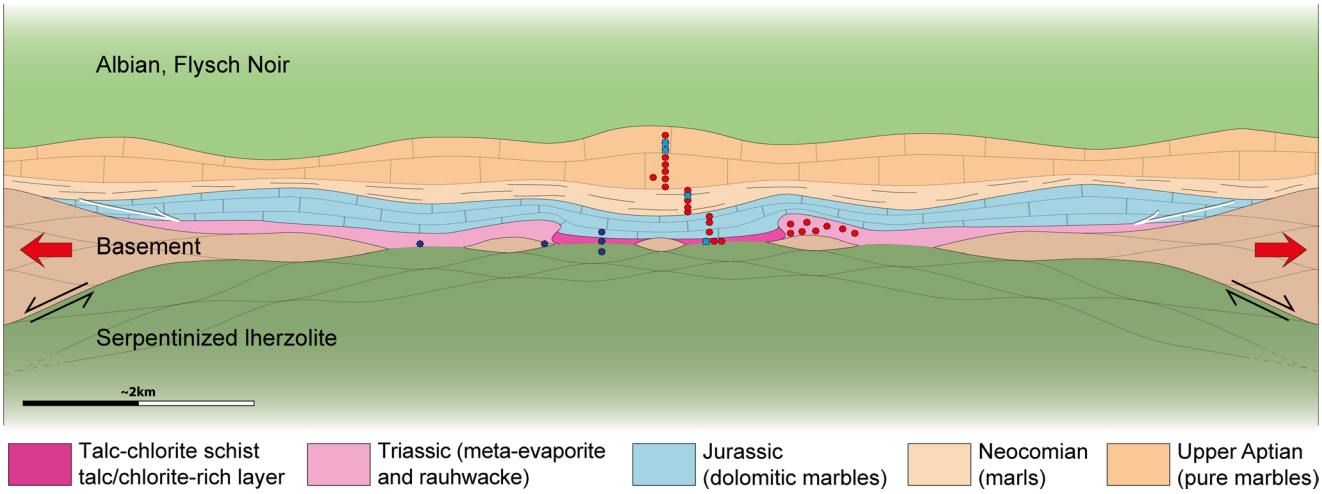

Fig. 4 Conceptual cross-section model based on field observations in the Saraillé massif showing the Albo-Cenomanian situation of the distal, hot passive margin with mantle exhumation (Corre et al. 2016) and replaced locations of studied samples (red and blue dots)

flattened in the foliation and forming the Saraillé summit. The Albian sequence includes an alternation of black marls, silts and limestones, known as the "Flysch Noir" (Roux 1983; Souquet et al. 1985; Debroas 1990; Corre et al. 2016).

Fluid-rock interactions and transformation of former protoliths

The Saraillé massif exposures display numerous evidence of infiltration by geological fluids and subsequent fluid-rock interactions revealing deep transformations of former protoliths. Calcite veins are abundant and distributed throughout the carbonate section of the Saraillé fold, above the talc-chlorite-rich layer. Quartz grains occur locally in veins. Dolomite and marble layers display a dense network of finely dispersed calcite veins, ranging 1–10 mm in thickness. In the phyllite-rich marbles, veins are less abundant but more concentrated. Most of the veins are randomly oriented, however by place some groups of veins display similar orientations. Locally, some veins are deformed by small shear zones. In the foliated marbles, veining may parallel and cross-cut the S0/S1 foliation (Fig. 5) (Corre et al. 2016).

The base of the metasedimentary pile is affected by an almost complete dolomitization. The limit between the dolomitic marbles and the calcitic marbles is characterized by a dolomitization front well observed in Jurassic rocks in the hinge of the Saraillé recumbent fold (Site A, Figs. 3 and 6). At this place, the base of the Aptian beds also shows dolomitization which is relatively rare in the NPZ. Such important dolomitization is not common in Mesozoic platform carbonates of Tethyan regions. We thus suspect that the dolomitic rocks exposed here have likely undergone dolomitization because of the specific geological history of the region, marked by exhumation of mantle rocks and related fluid circulation (Früh-Green et al. 2004).

An obvious proof of fluid circulation is the presence of a layer of metasomatic rocks preserved all along the mantle rocks/metasediments detachment fault and well exposed on the west flank of the Saraillé (Site B, Fig. 3). This layer is composed of strongly foliated talc-chlorite schists forming tens of meters thick rock lenses, exhibiting an uncommon pink colour (Fig. 7a). The foliation dips gently to the NE and parallels the detachment fault. Dolomite grains and pyrite crystals are aligned in the foliation. Some late veins of dolomite + pyrite crosscut the foliation (Fig. 7b). North of Site B, talc-chlorite schists progressively change to a yellowish color and include several fragments of cataclastic dolomites and mantle rocks transformed to talc but preserving the protolith texture (Fig. 7c, BCOR 108). Near the Laünde pass, the talc-chlorite schist layer laterally joins the Triassic sequence forming the core of the Sarrance anticline (Fig. 3a).

An important issue is the reconstruction of the original thickness and lithology of the pre-rift sequence before its strong attenuation during mantle exhumation. Lagabrielle et al. (2010) already pointed to the systematic allochtonous character of the Triassic rocks in the NPZ and to their intense mineralogical transformation during the HT-LP, syn-extensional metamorphic event. The Keuper metasediments of the Sarrance anticlinal are intensely sheared and constitute a tectonic melange, which incorporated tectonic clasts of micaschist, gneiss, ophite, dolomitic marble and rhauwacke in a matrix of talc and chlorite. This makes it difficult to establish the original stratigraphy and thickness of the Triassic deposits here (Castéras 1970; Lagabrielle et al. 2010). The presence of double-terminated quartz crystals (Fig. 7d, e) is generally accepted to indicate the (possibly former) occurrence of evaporitic rocks in the here described sequence (see e.g. Tarr 1929).

Generally, Upper Keuper deposits of the Pyrenees area consists of red, grey, and black shales, marls, and evaporites

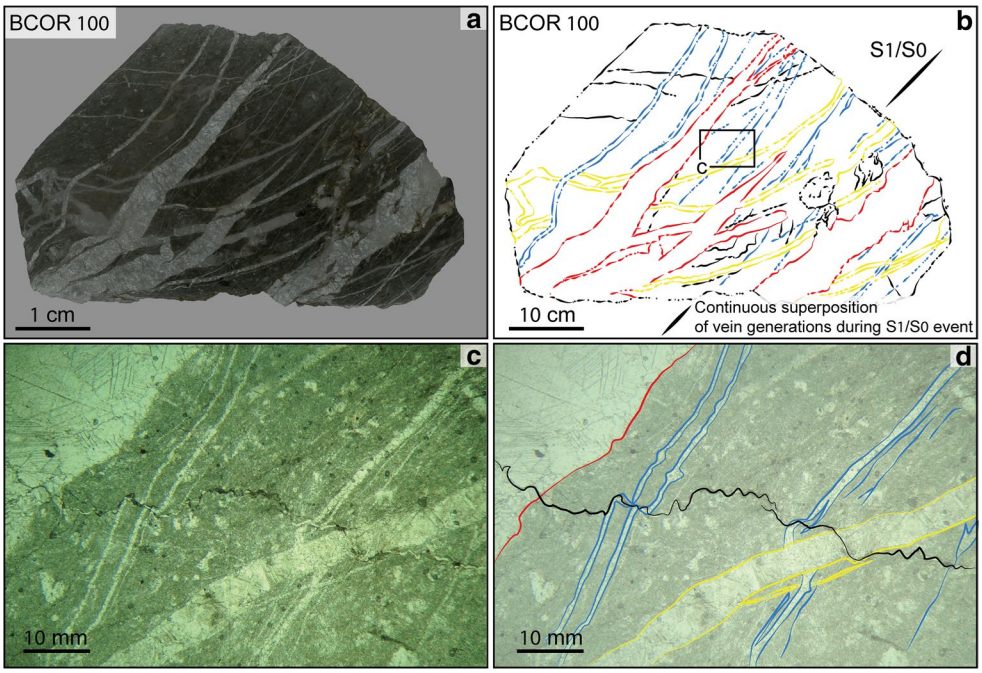

Fig. 5 **a** Picture of double polished thin-section of BCOR 100. **b** Interpretation of veining superposition of (**a**) **c** Thin section of BCOR 100 in LPNA, see location in (**b**) **d** Interpretation of veining superposition of picture **c**

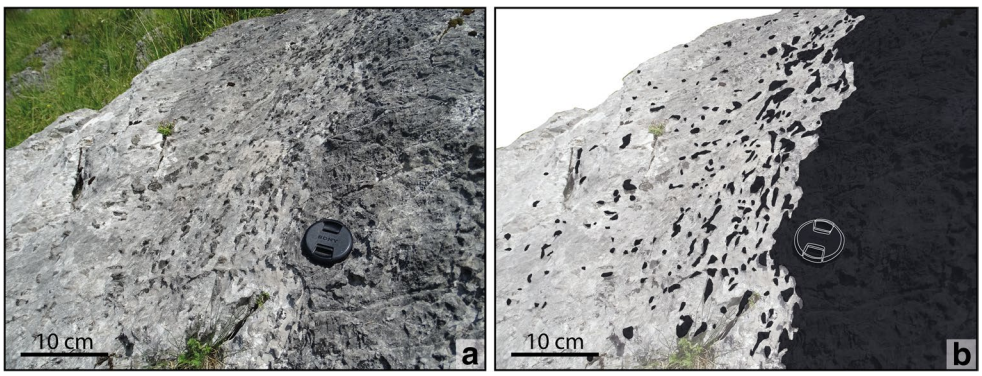

Fig. 6 Outcrop picture and its interpretation of a diffuse dolomitization front of the Site A, see Fig. 3 for location. In b, redrawn outcrop picture with pure marble in white and dolomitic marble in black

(gypsum, halite and anhydrite) (Salvany 1990; Flinch and Casas 1996; Calvet et al. 2004; Saura et al. 2015). In the Chaînons Béarnais, Canérot et al., (2005) deduced an original Keuper thickness of about 1650 m using a restoration approach. In the South and North Pyrenees, in the Bay of Biscay and in the Aquitaine basin, Keuper formations thickness varies from 0 to 2250 m (Lanaja et al. 1987; Biteau et al. 2006; Jammes et al. 2010; Roca et al. 2011; Saura et al. 2015).

Sampling strategy

Thirty-five samples have been collected from the Saraillé massif itself and from the core of the Sarrance anticline, in two separate sets during a reconnaissance campaign in 2007 (SAR samples) and a dedicated campaign in 2014–2015 (BCOR samples). In the latter, we sampled the lithologies affected by metasomatic processes at an increasing distance from the detachment fault presented by a talc-chlorite layer (Figs. 3 and 4). Where possible, both veins and host rocks were sampled. A sample description is presented in Table 1.

SAR samples

SAR samples include: (1) ultramafic and continental basement rocks, (2) the talc-chlorite schist layer in the detachment fault and (3) metasediments close to it. Mantle rocks are represented by highly serpentinized lherzolite (sample SAR 2d), whereas continental basement is represented by a chloritite sample (sample SAR 13). The metasomatic rocks are represented by the pink talc-chlorite schist (samples SAR 8 and SAR 30). The metasediments include Triassic cataclasites (sample SAR 17b) and Jurassic dolomitic marbles (samples SAR 10b, SAR 11a). Chemical analyses of the chlorite contained in these samples aimed

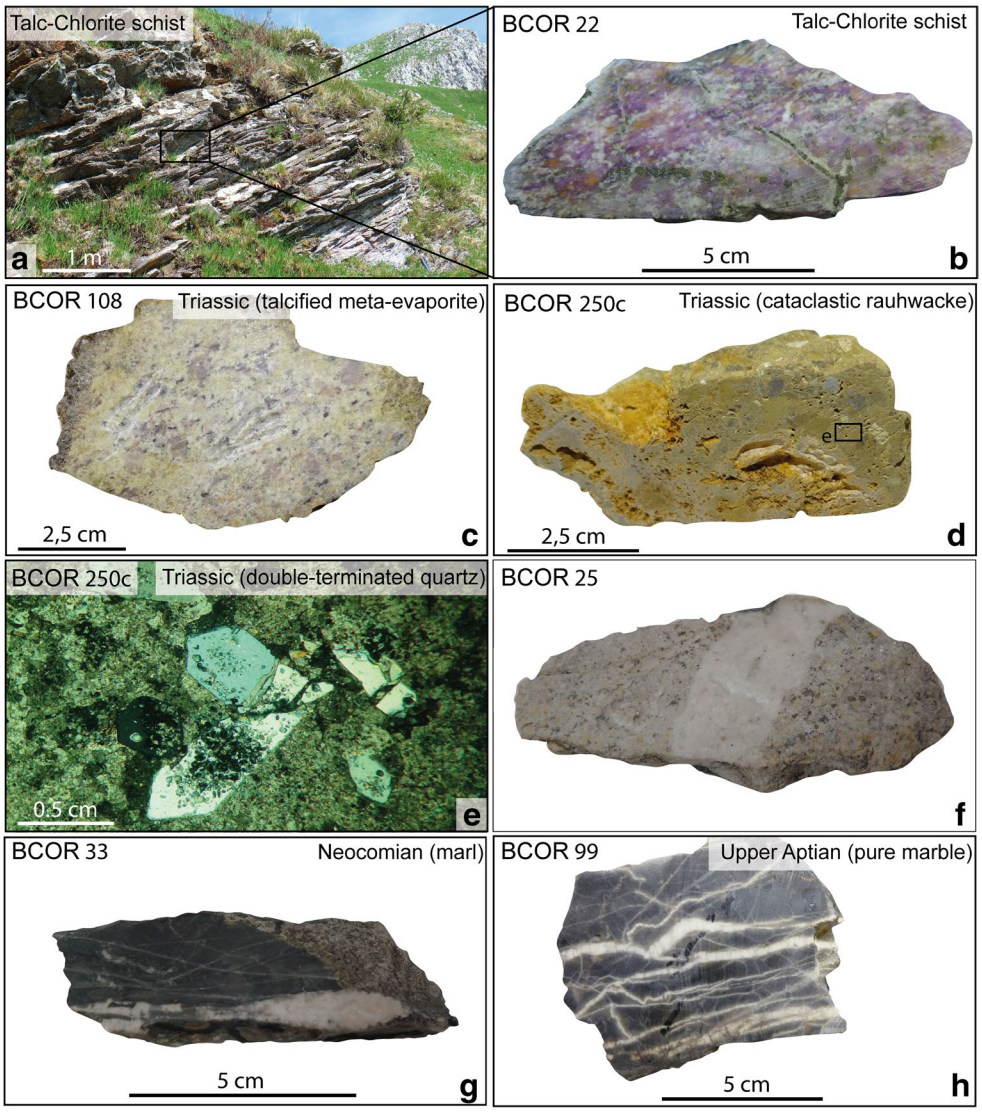

Fig. 7 Outcrop pictures of the Saraillé massif and selected hand-size samples and thin section of rocks from the Mesozoic métasédiments (see Fig. 2 for locations). **a** Foliated talc-chlorite schist. **b** Talc-chlorite schist (Sample BCOR 22) crosscut by millimetre dolomite-pyrite veins. **c** Sample Triassic talcified meta-evaporite (BCOR 108). **d** Polygenetic cataclastic rauhwacke (Sample BCOR 250c) of Triassic metasediments. **e** Thin section with double-terminated quartz within carbonate matrix (sample BCOR 250c). **f** Jurassic dolomitic marble (Sample BCOR 25) crosscut by centimetre carbonate vein. **g** Neocomian marl (Sample BCOR 33) with millimetre and centimetre veins. **h** Upper Aptian pure marble (Sample BCOR 99) showing flattening of different populations of carbonate veins parallel to or cutting the foliation

to characterize the metamorphic conditions using chlorite thermometry (Bourdelle and Cathelineau 2015) and at tracking the input of mantle-derived elements (Cr).

BCOR samples

The BCOR samples have been used for the fluid inclusions characterization and the O, C and Sr isotope analyses.

(a) The talc-chlorite metasomatic layer was sampled in three locations along the well exposed southwest flank of the Saraillé massif (samples BCOR 22, BCOR 23 and BCOR 24, Site B in Figs. 3 and 7a, b). These samples are a few meters away from each other. We collected five additional samples of talc-chlorite schists along the northern flank of the Saraillé massif (samples BCOR 107, BCOR 108 (Fig. 7c), BCOR 109, BCOR 110 and BCOR 249, Site C in Fig. 3a). These samples are strongly deformed with a well-developed schistosity and consist of an assemblage of talc and chlorite in variable proportions. They contain grains of Cr-rutile, dolomite and pyrite. The two latter minerals are also encountered in veins cutting through the talc-chlorite schists (Fig. 7b). Three additional samples of Triassic rocks were collected in the core of Sarrance anticline (Site C in Fig. 3a: samples BCOR 250b, c, e). These rocks are polymictic cataclasites composed of clasts of brown cellular dolomite, metaophites and Paleozoic schists in a fine-grained matrix of chlorite and talc including bipyramidal quartz (Fig. 7d, e).

(b) Sampling of the Mesozoic metasedimentary sequence was performed on the northwestern crest of the Saraillé massif. Samples BCOR 25, BCOR 27 and BCOR 28 are Jurassic fine-grained dolomitic marbles (Fig. 7f). They display a network of millimetric cal-

Table 1 Sample description of SAR and BCOR field campaigns

Sample	Type	Texture	Veins	Formation	Coordinates		Performed analyses
					Latitude	Longitude	
SAR 2d	Serpentinite	Talcified, foliated mantle rocks	Not present	Altered peridotite	*43°03′25″ N*	*00°38′42″ W*	*EPMA*
SAR 8	Talc-chlorite schist	Foliated, talcified	Some isolated veins oblique to S0/S1 (dolomite + pyrite)	Trassic (?)	*43°03′23″ N*	*00°38′47″ W*	*EPMA*
SAR 30	Talc-chlorite schist	Foliated, talcified	Some isolated veins oblique to S0/S1 (dolomite + pyrite)	Trassic (?)	*43°03′23″ N*	*00°38′47″ W*	*EPMA*
SAR 13	Chloritite	Foliated	Not present	Altered micaschist	*43°03′13″ N*	*00°38′28″ W*	*EPMA*
SAR 10b	Dolomitic marble	Foliated	Dense network of mm-veins (dolomite + pyrite)	Jurassic	*43°03′13″ N*	*00°38′28″ W*	*EPMA*
SAR 11a	Dolomitic marble	Foliated	Dense network of mm-veins (dolomite + pyrite)	Jurassic	*43°03′13″ N*	*00°38′28″ W*	*EPMA*
SAR 17b	Meta-evaporite	Brecciated	Not present	Triassic	*43°03′28″ N*	*00°38′39″ W*	*EPMA*
BCOR 22	Talc-chlorite schist	Foliated, talcified	Some isolated veins oblique to S0/S1 (dolomite + pyrite)	Trassic (?)	43°03′23″ N	00°38′47″ W	*SI and FI*
BCOR 23	Talc-chlorite schist	Foliated	One isolated cm-vein (dolomite)	Trassic (?)	43°03′23″ N	00°38′47″ W	*SI*
BCOR 24	Talc-chlorite schist	coarse-grained, weakly foliated	One isolated cm-vein (dolomite)	Trassic (?)	43°03′23″ N	00°38′47″ W	*SI*
BCOR 107	Talcschist	Talcified, foliated mantle rocks	Not present	Trassic (?)	43°03′23″ N	00°38′22″ W	*SI*
BCOR 108	Talcschist	Talcified, foliated mantle rocks	Not present	Trassic (?)	43°03′23″ N	00°38′22″ W	*SI*
BCOR 109	Talcschist	Brecciated, talcified	Not present	Trassic (?)	43°03′26″ N	00°38′15″ W	*SI*
BCOR 110	Talcschist	Foliated, talcified	Not present	Trassic (?)	43°03′26″ N	00°38′15″ W	*SI*
BCOR 249	Talcschist	Brecciated, talcified	Not present	Triassic	43°03′27″ N	00°38′15″ W	*SI*
BCOR 250b	Cataclasite	Brecciated	Not present	Triassic	43°03′10″ N	00°37′53″ W	*SI*
BCOR 250c	Cataclasite	Brecciated	Not present	Triassic	43°03′10″ N	00°37′53″ W	*SI*
BCOR 250e	Cataclasite	Brecciated	Not present	Triassic	43°03′10″ N	00°37′53″ W	*SI*
BCOR 25	Dolomitic marble	coarse-grained, weakly foliated	One isolated cm-vein (dolomite), disseminated talc	Jurassic	43°03′23″ N	00°38′47″ W	*SI and FI*
BCOR 27	Dolomitic marble	Fine-grained	Dense network of mm-veins (calcite)	Jurassic	43°03′23″ N	00°38′47″ W	*SI and FI*
BCOR 28	Dolomitic marble	Fine-grained	Dense network of mm-veins (calcite)	Jurassic	43°03′23″ N	00°38′45″ W	*SI*
BCOR 30	Pure marble	Fine-grained	Dense network of mm-veins (calcite)	Neocomian	43°03′23″ N	00°38′44″ W	*SI*
BCOR 31	Pure marble	Fine-grained	Dense network of mm-veins (calcite)	Neocomian	43°03′23″ N	00°38′43″ W	*SI*
BCOR 32	Phyllite-rich marble	Fine grained foliated	One isolated mm-vein, oblique to S0/S1 (calcite)	Neocomian	43°03′22″ N	00°38′42″ W	*SI*
BCOR 33	Phyllite-rich marble	Fine grained weakly foliated	Dense network of random mm-vein and one isolated cm-vein oblique to S0/S1 (calcite)	Neocomian	43°03′22″ N	00°38′41″ W	*SI and FI*

Table 1 (continued)

Sample	Type	Texture	Veins	Formation	Coordinates		Performed analyses
					Latitude	Longitude	
BCOR 34	Phyllite-rich marble	Fine grained foliated	One isolated mm-vein, oblique to S0/S1 (calcite)	Neocomian	43°03′20″ N	00°38′40″ W	*SI*
BCOR 35	Phyllite-rich marble	Fine grained weakly foliated	Some isolated veins oblique to S0/S1 (calcite)	Neocomian	43°03′20″ N	00°38′36″ W	*SI*
BCOR 36	Pure marble	Recristallized	Dense network of mm-veins (calcite)	Upper Aptian	43°03′20″ N	00°38′39″ W	*SI*
BCOR 92a	Calcite	Mono-crystal	Calcite	Upper Aptian	43°03′10″ N	00°38′53″ W	*SI*
BCOR 92b	Calcite	Mono-crystal	Calcite	Upper Aptian	43°03′10″ N	00°38′53″ W	*SI*
BCOR 96	Pure marble	Recristallized	Dense network of mm-veins (calcite)	Upper Aptian	43°03′19″ N	00°38′37″ W	*SI*
BCOR 97	Pure marble	Recristallized	Dense network of mm-veins (calcite), stylotiths	Upper Aptian	43°03′19″ N	00°38′36″ W	*SI*
BCOR 98	Pure marble	Recristallized	Dense network of mm- and cm-veins (calcite)	Upper Aptian	43°03′18″ N	00°38′35″ W	*SI*
BCOR 99	Pure marble	Recristallized	Dense network of mm-veins parallel to S0/S1 (calcite)	Upper Aptian	43°03′17″ N	00°38′34″ W	*SI and FI*
BCOR 100	Pure marble	Recristallized	Dense network of mm- and cm-veins (calcite)	Upper Aptian	43°03′14″ N	00°38′32″ W	*SI and FI*
BCOR 101	Pure marble	Recristallized	Dense network of mm-veins, random orientation (calcite)	Upper Aptian	43°03′12″ N	00°38′30″ W	*SI and FI*

citic veins and close to the talc-chlorite schist, they include up to 20% disseminated talc, chlorite and pyrite crystals. Samples BCOR 30–35 are Neocomian calcitic marbles and phyllite-rich calcitic marbles (Fig. 7g). The amount of phyllite grains causes the marbles to vary in colour from light grey to dark grey. In the phyllite-rich marbles, veins are less abundant than in pure calcitic marbles. Lastly, samples BCOR 36–101 are Aptian pure calcitic marbles (Fig. 7h). A network of abundant mm- to cm-thick calcite veins is observed in all samples. Locally, veins exhibit a diffuse contact with host rock. Sample BCOR 92 consists of a 50 cm-thick vertical calcite vein a few meters long (Fig. 3a, b).

Analytical techniques

Preparation of polished sections

Polished sections of standard size ~ 28 × 48 mm were prepared by Thin Section Lab at Toul/FR (http://www.thinsectionlab.com) using a routine procedure. Sample were cut to billets ~ 10 × 30 × 45 mm with a water-cooled diamond blade, and after drying impregnated with a colorless single-component organic binder cured at 60–80 °C. The billets main surfaces were dressed planar on bonded diamond discs from 80 to 600 mesh, and finished 800 mesh carborundum slurry. The prepared face was mounted to a carrier glass with Araldite® cured at 40–60 °C, excess sample material was cut off with a diamond saw to ~ 0.5 mm, and the mounted section lapped to 30–35 µm thickness again with 800 mesh carborundum slurry. Finally, the prepared surface was polished in four successive steps with diamond pastes of 6-3-1-0.25 µm fineness. Preparation of double polished sections for fluid inclusion studies introduces an additional polishing stage prior to mounting on the carrier glass.

Electron-probe micro-analysis - EPMA

The chemical compositions of chlorite, talc and dolomite in seven SAR samples from the talc/chlorite layer were analysed at the Service Commun de Microsonde Ouest

(SCMO, Plouzané, France), using a CAMECA SX100 microprobe, operated at 15 kV, 20nA, spot size 5 µm and 10 s counting time on peak and 5 s on background. The EPMA instrument was equipped with five WDS detectors with LIF, PET, and TAP crystals, and all elements were assigned to specific detectors to be measured 5 + 5 concurrently per run of ~ 30 s total duration. Standards were natural albite (Na, Si), orthoclase (K), corundum (Al), wollastonite (Ca), forsterite (Mg), MnTiO3 (Mn, Ti), andradite (Fe) and chromite (Cr). Raw spectral data were ZAF-corrected using the phi-rho-Z protocol of Pouchou and Pichoir (1984) known as 'PAP'. Element contents were recalculated to oxides by stoichiometry, total iron content is represented as FeO. Limits of detection are: 0.01 wt% (Mn, Ti, Fe, Cr), 0.05 wt% (Ca, Si, K) and 0.10 wt% (Al, Mg, Na). Main element oxide contents in wt% were recalculated into mineral compositions in atoms per formula unit – apfu using standard routines (Tables 2, 3 and 4). Volatiles contents in H_2O and/or CO_2 were calculated by balance of the sum total with 100.00 wt%. Mineral names are abbreviated according to recommendations by Whitney and Evans (2010).

Fluid inclusions studies

Fluid inclusions were studied at the GeoRessources laboratory, University of Lorraine (Nancy) on double polished thin sections from eight samples. Micro-thermometric measurements were performed on wafers using a Linkam heating – cooling stage mounted on an Olympus BX-61 microscope. A Dilor-Labram RAMAN micro-spectrometer was used for the quantitative measurements of the gas species present in the fluid inclusions following the procedure described by Dubessy et al. (1989).

Assessment of carbon and oxygen stable isotope ratios

Stable isotope ratios of $^{12}C/^{13}C$ and $^{16}O/^{18}O$ were measured at the stable isotope laboratory of Geosciences Rennes, University of Rennes 1. Sample powder was recovered by micro-drilling of diamond-cut faces in hand specimen. About 12 mg of powdered carbonate was reacted with anhydrous phosphoric acid (H_3PO_4) for a few hours at 50 °C in order to liberate CO_2 (McCrea 1950). Isotopic

Table 2 Average compositions (AVG) and standard deviations (SD) by electron-probe micro-analyses – EPMA in weight percent [wt%], of chlorite from base tectonic contact lithologies, and numbers of cations in atoms per formula unit – apfu calculated using standard protocol. FeO-total represents total iron content, water content calculated by balance with 100.0 wt%

	Lithology SAR (#analyses)	Serpentinite 2d (n = 5)		Chlorite-talcschist 8 & 30 (n = 5)		Chloritite 13 (n = 18)		Dolostone (J.) 10b & 11a (n = 18)		Meta-evaporite (Tr.) 17b (n = 2)	
	LLD	AVG	SD	AVG	SD	AVG	SD	AVG	SD	AVG	SD
SiO_2	0.05	33.3	4.36	35.7	1.21	31.6	0.70	31.8	0.73	31.6	0.64
TiO_2	0.01	0.13	0.12	0.02	0.01	0.08	0.23	0.03	0.03	0.05	0.04
Al_2O_3	0.10	12.4	2.34	13.2	0.86	19.5	0.87	17.8	1.80	16.5	0.12
Cr_2O_3	0.01	3.38	4.14	1.44	0.65	0.05	0.15	1.68	0.47	1.32	0.14
FeO-total	0.01	5.78	1.89	0.02	0.03	1.97	1.91	2.34	2.36	4.72	1.07
MnO	0.01	0.08	0.09	0.01	0.02	0.05	0.07	0.04	0.03	0.02	0.02
MgO	0.10	32.5	2.70	35.9	0.59	32.3	1.57	32.1	1.27	31.5	0.42
CaO	0.05	0.02	0.02	0.01	0.01	0.04	0.03	0.04	0.02	< 0.01	–
Na_2O	0.10	0.02	0.02	0.01	0.02	0.02	0.02	0.01	0.01	0.03	0.01
K_2O	0.05	0.01	0.01	0.02	0.02	0.02	0.01	0.01	0.01	< 0.01	–
SUM	–	87.6	1.39	86.4	0.77	85.5	1.82	85.8	0.62	85.8	0.03
H_2O	calc	12.4	–	13.6	–	14.5	–	14.2	–	14.2	–
Numbers of cations in apfu, based on 10O + 4OH											
Si	–	3.18	0.39	3.33	0.07	2.99	0.04	3.03	0.08	3.05	0.04
Ti	–	0.01	0.01	0.00	0.00	0.01	0.02	0.00	0.00	0.00	0.00
Al	–	1.39	0.26	1.45	0.10	2.18	0.07	1.99	0.18	1.87	0.00
Al (IV)	–	0.82	0.39	0.67	0.07	1.01	0.04	0.97	0.08	0.95	0.04
Al (VI)	–	0.57	0.14	0.78	0.10	1.17	0.05	1.02	0.12	0.93	0.04
Cr	–	0.26	0.31	0.11	0.05	0.00	0.01	0.13	0.04	0.10	0.01
Fe-total	–	0.46	0.15	0.00	0.00	0.16	0.15	0.19	0.19	0.38	0.09
Mn	–	0.01	0.01	0.00	0.00	0.00	0.01	0.00	0.00	0.00	0.00
Mg	–	4.61	0.36	4.99	0.10	4.56	0.16	4.56	0.12	4.54	0.03
SUM	–	9.92	0.08	9.89	0.05	9.91	0.03	9.91	0.03	9.96	0.04

Numbers of cations [apfu] for Ca, Na, and K all < 0.01 (not listed)

Table 3 Average compositions (AVG) and standard deviations (SD) by electron-probe microanalyses – EPMA in weight percent [wt%], of talc from base tectonic contact lithologies, and numbers of cations in atoms per formula unit – apfu calculated using standard protocol. FeO-total represents total iron content, water content calculated by balance with 100.0 wt%

	Lithology SAR (#analyses)	Serpentinite 2d (n = 2)		Chlorite-talcs-chist 8 & 30 (n = 15)		Dolostone (J.) 10b & 11a (n = 5)		Meta-evaporite (Tr.) 17b (n = 12)	
	LLD	AVG	SD	AVG	SD	AVG	SD	AVG	SD
SiO_2	0.05	61.5	0.52	62.5	1.80	61.6	1.32	62.0	0.72
TiO_2	0.01	0.02	0.02	0.02	0.03	0.12	0.11	0.02	0.02
Al_2O_3	0.10	0.64	0.04	0.55	0.81	0.71	0.60	0.15	0.09
Cr_2O_3	0.01	0.01	0.00	0.05	0.15	0.18	0.18	0.09	0.05
FeO-total	0.01	1.24	0.11	0.11	0.20	2.38	1.39	2.07	0.08
MnO	0.01	0.01	0.02	0.01	0.01	0.01	0.01	0.02	0.02
MgO	0.10	30.9	0.27	31.8	0.55	29.8	0.74	29.0	0.90
CaO	0.05	0.02	0.02	0.02	0.02	0.03	0.02	0.09	0.16
Na_2O	0.10	0.05	0.04	0.01	0.02	0.06	0.03	0.04	0.02
K_2O	0.05	0.03	0.02	0.01	0.01	0.02	0.01	0.02	0.02
SUM	–	94.5	0.73	95.1	0.65	94.9	0.34	93.5	0.94
H_2O	calc	5.5	–	4.9	–	5.1	–	6.5	–
Numbers of cations in apfu, based on 10O + 2OH									
Si	–	3.95	0.00	3.96	0.08	3.95	0.06	4.02	0.04
Ti	–	0.00	0.00	0.00	0.00	0.01	0.01	0.00	0.00
Al	–	0.05	0.00	0.04	0.06	0.05	0.05	0.01	0.01
Cr	–	0.00	0.00	0.00	0.01	0.01	0.01	0.00	0.00
Fe-total	–	0.07	0.01	0.01	0.01	0.13	0.07	0.11	0.00
Mg	–	2.96	0.00	3.01	0.07	2.85	0.06	2.80	0.07
Ca	–	0.00	0.00	0.00	0.00	0.00	0.00	0.01	0.01
Na	–	0.01	0.00	0.00	0.00	0.01	0.00	0.00	0.00
SUM	–	7.03	0.00	7.02	0.05	7.01	0.03	6.97	0.04

Numbers of cations [apfu] for Mn and K all < 0.01 (not listed)

rations were measured on a VG OPTIMA triple collector mass spectrometer. Samples of reference material NBS 18 and internal-laboratory standard Prolabo Rennes were inserted throughout the sample series for internal calibration. NBS 18 values (n = 2) were $\delta^{18}O = 6.90 \pm 0.05‰$ (vs. SMOW) and $\delta^{13}C = -5.06 \pm 0.007‰$ (vs. PDB), close to the recommended values at 6.94 and −5.01‰, respectively. Internal-lab standard measured values (n = 7) were $\delta^{18}O = 11.26 \pm 0.12‰$ (vs SMOW) and $\delta^{13}C = -9.68 \pm 0.02‰$ (vs PDB), also these in good agreement with long-term average values of 11.16 and −9.69‰, respectively. Isotopic compositions for the samples were corrected according to the results for the internal standards. The analytical precision is estimated at ±0.20‰ for O and ±0.10‰ for C. Some Triassic metasediments and talc-chlorite schists were treated by selective extractions to get the isotopic compositions of both dolomite and calcite fractions present in the rocks. The CO_2 liberated after 2 h of reaction at 25 °C was assumed to derive from digested calcite CaCO3, and was extracted for analysis. After a minute of pumping, the vessel was heated at 50 °C in a hot bath until complete reaction (the latter CO_2 fraction was ascribed as dolomite-derived).

Strontium isotopes

For analysis of Sr isotopes, sample materials were extracted by micro-drilling from cut faces in hand specimen in the same way as for C, O-stable isotope extraction. About 50–100 mg of calcite powder was digested in 2.5N HCl at room temperature for 1 h. Less soluble dolomite was digested in 6N HCl instead, in otherwise identical conditions. Extracts were ion-exchanged in an Ion BioRad column to concentrate Sr. Strontium isotopes were analyzed on a Finnegan MAT 262 multi-collector mass spectrometer.

Results

Mineral compositions

Average compositions and corresponding structural formula of chlorite, talc and dolomite grains from SAR samples are presented in Tables 2, 3 and 4.

Chlorites have a clinochlore composition. The Al content is lower in the serpentinite and in the talc-chlorite schists than in the Mesozoic rock, especially in the chloritite sample SAR

Table 4 Average compositions (AVG) and standard deviations (SD) by electron-probe micro-analyses – EPMA in weight percent [wt%], of dolomite from base tectonic contact lithologies, and numbers of cations in atoms per formula unit – apfu calculated using standard protocol. FeO-total represents total iron content, ignition loss – LOI calculated by balance with 100.0 wt%

	Lithology SAR (#analyses)	Chlorite-talcschist 8 & 30 (n = 4)		Dolostone (J.) 10b & 11a (n = 12)		Meta-evaporite (Tr.) 17b (n = 8)	
	LLD	AVG	SD	AVG	SD	AVG	SD
SiO_2	0.05	< 0.02	–	0.12	0.25	0.02	0.02
TiO_2	0.01	0.01	0.01	0.03	0.03	0.01	0.02
Al_2O_3	0.10	0.02	0.01	0.04	0.09	0.01	0.01
Cr_2O_3	0.01	< 0.01	–	< 0.01	–	< 0.01	–
FeO-total	0.01	0.02	0.01	0.07	0.13	2.11	0.18
MnO	0.01	0.10	0.02	0.11	0.07	0.06	0.03
MgO	0.10	22.2	0.36	21.0	0.94	19.4	0.26
CaO	0.05	30.5	0.24	30.8	0.56	29.5	0.13
Na_2O	0.10	0.01	0.01	0.02	0.02	0.01	0.01
K_2O	0.05	0.01	0.01	0.01	0.01	< 0.01	–
SUM	–	52.8	0.41	52.2	1.25	51.1	0.22
LOI	calc	47.2	–	47.8	–	48.9	–
Numbers of cations in apfu, based on 6O							
Si	–	0.00	0.00	0.00	0.01	0.00	0.00
Fe-total	–	0.00	0.00	0.00	0.00	0.06	0.01
Mg	–	1.00	0.01	0.96	0.02	0.93	0.01
Ca	–	0.99	0.01	1.02	0.03	1.01	0.01
SUM	–	2.00	0.00	2.00	0.01	2.00	0.00

Numbers of cations [apfu] for Ti, Al, Mn, Cr, Na and K all < 0.01(not listed)

13 (Tables 2, 3, 4). Conversely, the Cr_2O_3 content is maximal in the serpentinites and varies between 1.3 and 1.7 wt%. The chlorite compositions are reported in the Si versus R^{2+}diagram of Wiewióra and Weiss (1990) calculated with the thermometer of Bourdelle and Cathelineau (2015) (Fig. 8); the estimated temperatures of chlorite formation are between ~ 150 °C and ~ 300 °C.

Talc composition is the closest to theoretical composition in the talc-chlorite schist. In the other lithologies, the FeO content, as an example, varies between 1.2 and 2.4 wt%.

Dolomite composition is almost pure, except in the meta-evaporites were the FeO content reaches 2.1 wt%.

Fluid inclusions

Fluid inclusions were analysed on dolomite, quartz and calcite grains in eight carbonate veins (Table 5). Aqueous fluid inclusions are the most abundant. Most have a very small size (< 5µ m; Fig. 9a, b). In sample BCOR 33 (Fig. 9c, d), a solid cubic phase can be observed corresponding to halite. Homogenization temperatures measured are highly variable (from 40 to more than 300 °C) without a clear distinction between the lithologies that host the studied veins (Fig. 10a). The whole range actually corresponds to inclusions in calcite, a rather weak mineral in which inclusions may not be well preserved. The range defined by inclusions from dolomite (180–250 °C, mode near 210 °C) and from quartz (130–160 °C) are much more restricted. Salinity estimated from the ice melting temperatures ranges between 13 wt% and 34 wt% Eq. NaCl.

Raman spectroscopy allowed identifying traces of gas in the aqueous inclusions from calcite and quartz (samples BCOR 22 and BCOR 33). N_2 is dominant (> 90%) whereas CH_4 is minor (< 5%). In veins from samples BCOR 99 and BCOR 100, the dissolved species is H_2S, with no more N_2 nor CH_4.

Stable isotopes

Oxygen and carbon isotope compositions were determined on veins and host rocks (Table 6; Figs. 11 and 12). $\delta^{18}O$ and $\delta^{13}C$ values display large ranges from 11.6 to 25.8‰ (SMOW) and from − 5.9 to 3.6‰, respectively. None of our values are identical to those of unaltered marine limestones (Fig. 11). The calcite in the talc-chlorite schist is out of equilibrium with dolomite in both O and C systems (Table 6). Calcite in the Triassic levels also displays negative $\delta^{13}C$ values, for $\delta^{18}O$ values comparable to those of calcite in the talc-schist. These high $\delta^{18}O$ and low $\delta^{13}C$ values are highly suspected to correspond to meaningless post-metamorphic, low-temperature, carbonation (Alonso-Zarza 2003) and are thus not considered further. Focussing on the carbonate-rich lithologies, the $\delta^{18}O$ values regularly evolves with the distance to the detachment (Fig. 13a), the lowest values being

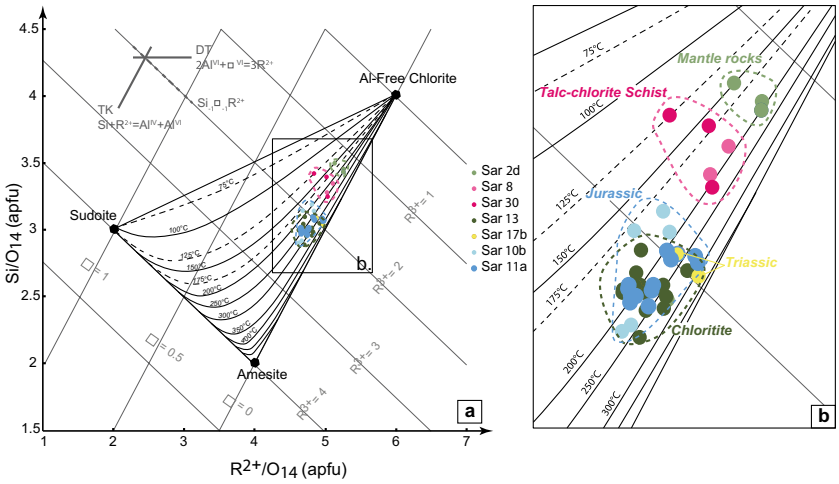

Fig. 8 **a** SiO_2 versus R^{2+} diagram applied to the compositions of the chlorites with indication of the temperature of crystallization obtained with the chlorite geothermometer from Bourdelle and Cathelineau (2015). The data are distinguished as a function of their lithologies. **b** Zoom on the data set

recorded by Upper Aptian calcitic marbles, at the summit of the Saraillé (geologically immediately below the Albian "Flysch Noir"). Veins and host rocks are in equilibrium in both O and C isotope systems all along the sampling profile (Fig. 13b), which is the sign of continuous equilibration between veins and local rocks, likely under variable fluid/rock ratios.

Strontium isotopes

The measured $^{87}Sr/^{86}Sr$ ratios are presented in Table 6 and Fig. 13c. On a first approximation, these values are likely well preserved and can be considered as representative of the original fluids because of the low Rb content expected for carbonates, i.e. no or very minor radiogenic growth of ^{87}Sr occurred since carbonate crystallization. A range between 0.70730 and 0.70846 is observed, the minimum value being recorded by Neocomian marbles and the maximum values by a talc-schist. The Upper Aptian rocks exhibit values higher than the marine Aptian limestones (Veizer et al. 1999). The two vein-host rock pairs analyzed for Sr isotopes display distinct characteristics. Vein and host rock have identical $^{87}Sr/^{86}Sr$ ratio in one case, clearly distinct in the other. Interestingly, the latter also displays some distinct values in the oxygen isotope system.

Discussion

Syn-kynematic fluid circulations

Most of the rocks that compose the limbs of the Saraillé fold have undergone interactions with fluids. Best evidence are as follows: (i) calcite veins are abundant and distributed throughout the carbonate section of the Saraillé fold, (ii) Aptian marbles are locally dolomitized, (iii) a thick layer of talc-chlorite schists, cross-cut itself by late carbonate veins, is recognized at the contact between mantle rocks and metasediments and (iv) the oxygen isotope composition of carbonate has been altered to values lower than those of their non-metamorphic counterparts. As reported above, the Keuper metasediments of the Sarrance anticline are intensely tectonized and constitute a tectonic mélange composed of clasts of various lithologies in a talc- and chlorite-rich matrix. Geological mapping has revealed that the Keuper level and the layer of metasomatic talc-chlorite schists are continuous (Corre et al. 2016). Both represent the rheological discontinuity along which localized the Mesozoic cover gliding and thus corresponds to the portion of the detachment that allowed mantle rocks to reach the shallowest levels of the crust during the Albian-Cenomanian extension.

From both macroscopic and microscopic observations of the veining in the Mesozoic sedimentary cover, it appears that fluids have circulated during the deformation of the sediments. Most of the veins are randomly oriented, but by place some groups of veins display similar orientation. Some veins are deformed by small shear zones (Figs. 6 and 7 h) and others are boudinaged and parallel the S0/S1 foliation (Figs. 6 and 7 g). Moreover, the S0/S1 foliation is parallel to the recumbent fold shape of the Saraillé (Corre et al. 2016). These observations imply that fluid circulation responsible for the intense network veining was maintained in the sedimentary cover during the entire period of its deformation. The O, C and Sr isotope equilibrium observed among most vein-host rock couple are consistent with this point, as well as the fact that the couples for which a small disequilibrium is observed in O and Sr (samples BCOR 25 and BCOR 27) are nearly free of deformation. At the scale of these samples, the isotopic values of the veins are then closer to the fluid end-member than to the rock end-member in a fluid-rock interaction system with varying fluid/rock ratio. The talc-chlorite schist layer locally contains clasts of dolomitic marbles. Some of them exhibit an internal micro-folded fabric indicative of an early ductile deformation that was

Table 5 Fluid inclusion characteristics of dolomites, calcites and quartz in the Mesozoic sedimentary sequence of the Saraillé Massif

Aqueous inclusions											
Dolomite				Calcite				Quartz			
Sample	Th (°C)	Salinity (%)	Gas species and liquid	Sample	Th (°C)	Salinity (%)	Gas species and liquid	Sample	Th (°C)	Salinity (%)	Gas species and liquid
BCOR 22 Talc-chlorite schist				BCOR 25 Jurassic				BCOR 33 Neocomian			
Range	185/239			Range	171.6/237			Range	135/156		H2O liquid
Mode	210	22–27	Salted H2O	Mode	210	nd	nd	Mode	140	32–34	CH4 gas (4%)
n	29			*n*	10			*n*	6		N2 gas (96%)
BCOR 25 Jurassic				BCOR 27 Jurassic							
Range	176/245			Range	87/215						
Mode	210	nd	nd			nd	nd				
n	3			*n*	3						
				BCOR 99A Aptian							
				Range	42/>320		Salted H2O liquid H2S liquid				
				Mode	250	15–17					
				n	18						
				BCOR 99B Aptian							
				Range	37.7/60		Salted H2O liquid H2S liquid and gas				
				Mode	50	17–20					
				n	6						
				BCOR 100 Aptian							
				Range	41/219		Salted H2O liquid H2S liquid				
				Mode	210	13–29					
				n	15						
				BCOR 101 Aptian							
				Range	110/166						
				Mode	120	nd	nd				
				n	5						

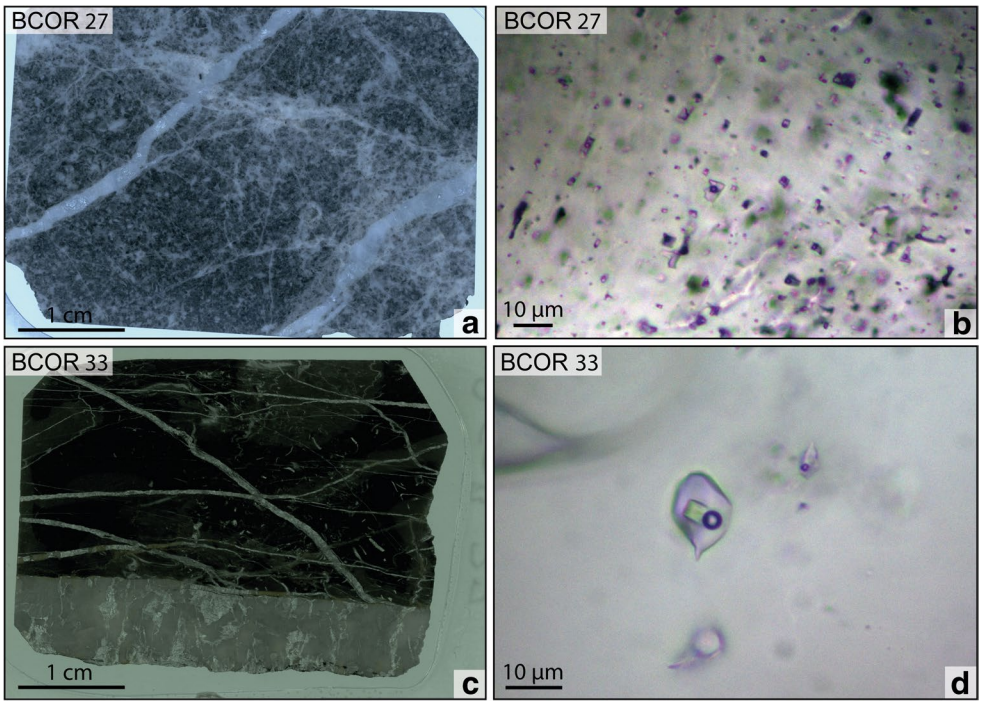

Fig. 9 Samples BCOR 27 and BCOR 33 analysed for fluid inclusions. **a** Picture of double polished thin-section of BCOR 27. **b** Two phase FIs in calcite from BCOR 27. **c** Picture of double polished thin-section of BCOR 33. **d** Three phase FIs in quartz from BCOR 33

necessarily acquired deeper along the detachment (Fig. 7a, b). This suggests that this metasomatic layer has grown by the aggregation of fragments of fault rocks that travelled along the detachment zone. These fragments were cemented by authigenic phyllitic minerals. In addition, some late veins of dolomite + pyrite crosscut the foliation of the talc-chlorite schists implying that a distinct fluid circulated during the last stages of the detachment fault activity, under more brittle conditions (Fig. 7b). These observations point to a complex history of fluid circulation in relation with the ascent of the mantle rocks. In the following, we aim to decipher some important steps of this history.

Evidence for competing metasomatic systems

At a broad scale, we can distinguish two metasomatic systems in the Saraillé massif. The first corresponds to the metasomatic, syn-kinematic, talc-chlorite schist formation at the base of the allochthonous sedimentary cover. The second one corresponds to the intense veining that dissects the entire Mesozoic cover, including the talc-chlorite schists. The detachment fault separating crustal and mantle basement rocks from the mobile sedimentary cover is a preferential pathway for fluid circulation. Increase in permeability of ductilely deforming rocks relative to adjacent less deformed rocks tends to focus fluid flow into the shear zone (Reynolds and Lister 1987). However, we can show that the fluids circulating in the detachment fault were not completely confined in the talc-chlorite layer. Indeed, talc and clinochlore are present in all the lithologies of the detachment fault: mantle rocks, Jurassic dolomitic marbles and Triassic metasediments (Table 1; Fig. 8). Therefore, ductile deformation within the detachment shear zone resulted in a large increase in dynamically maintained permeability within a detachment fault zone a few tens of meters thick (Urai 1983; Etheridge et al. 1983; Géraud et al. 1995; Sibson and Rowland 2003; Violay et al. 2015). The lowermost $\delta^{18}O$ values of carbonates in talc-schist are about 15–16‰ (Table 6). Considering (i) a temperature of alteration between 150 and 250 °C, (ii) a pure aqueous fluid (consistently with the fluid inclusion characterization) and (iii) the fact that the fluid circulated in large amounts, preserving its original signature, the $\delta^{18}O$ value of the detachment fluid can be estimated in the range 3–8‰. Such range is consistent with a fluid originally derived from seawater and which would have interacted with mantle rocks (the peridotites are indeed serpentinized and the rocks in the detachment have Cr-rich chlorites). The slight deviation of Sr isotopes from the theoretical value of seawater may be related to the incorporation of crustal radiogenic strontium during fluid migration at the mantle-crust interface, along the detachment.

The second fluid-rock interaction system is deduced from the isotopic evolution of carbonates along the sampling transect. The stable isotope analysis of the Saraillé carbonates shows that the most altered marbles, i.e. those with the lowest $\delta^{18}O$ values, are the Aptian marble beds located at the top of the metasedimentary pile (Fig. 13a). A value of around 12‰ is recorded by the vein-host rock pair at the top of the exposed metasedimentary series, but it is possible that even lower values would have been reached by the overlaying levels today disappeared through erosion. In the range of temperatures estimated for this second fluid-rock

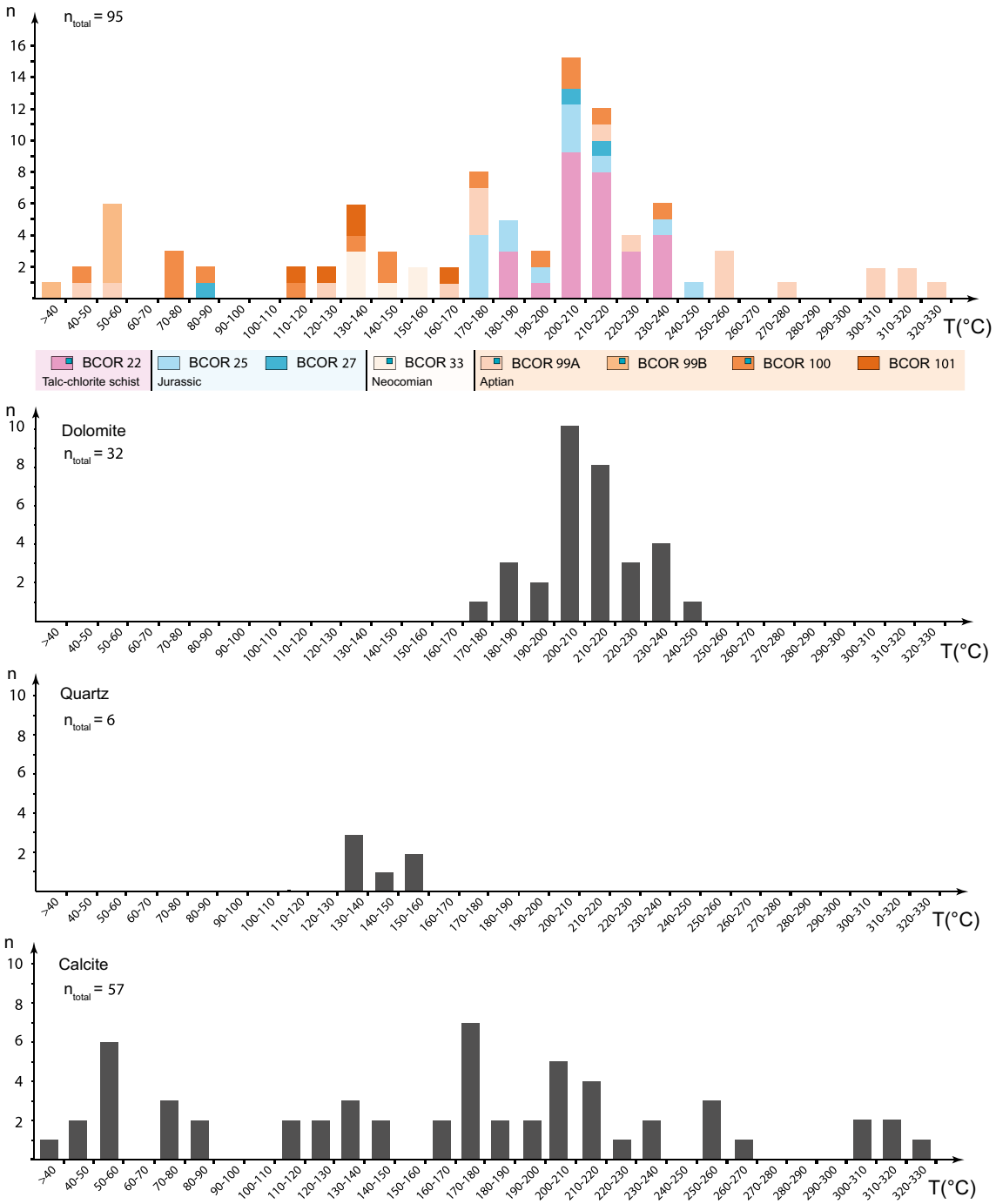

Fig. 10 Homogenization temperatures T_h histograms of analysed FIs. **a** All T_h analysis for all samples (blue squares represent the samples with three phase FIs). **b** T_h obtained in dolomite grains. **c** T_h obtained in quartz grains. d. T_h obtained in calcite grains

interaction system (200–300 °C, Fig. 8), the $\delta^{18}O$ value that can be expected for the infiltrating aqueous fluid (in the range 2,5–6,5‰) has to be considered as a maximum value. Such values are in agreement with those expected for salty aqueous fluids (salinities up to 34 wt.% eq. NaCl are recorded in some samples) that came from the deeper level where Triassic evaporites are dissolved. Mixing of such saline fluid with the first fluids documented along the detachment is supported by our data. Along the section, the progressive isotopic changes may then be attributed to an increase in fluid/rock ratio, with a larger volume of fluids circulating at the top of the sedimentary section. Boulvais et al. (2006) proposed such a varying fluid/rock ratio for the isotopic trend recorded in the Trimouns/ La Porteille talc

Table 6 O and C isotope compositions of the Mesozoic sedimentary sequence of the Saraillé Massif

				Calcite		Dolomite		
	Sample	Type		$\delta^{18}O$ (‰)	$\delta^{13}C$ (‰)	$\delta^{18}O$ (‰)	$\delta^{13}C$ (‰)	$^{87}Sr/^{86}Sr \pm 10^{-6}$
Talc-chlorite schist	BCOR 22	Talc-chlorite schist	HR			19	1.8	0.708247 ± 14
			Vein			19	1.9	
	BCOR 23	Talc-chlorite schist	HR			19	1	0.708461 ± 12
	BCOR 24	Talc-chlorite schist	HR			19.7	1.9	
	BCOR 107	Talcschist	HR			15.3	1.2	
	BCOR 108	Talcschist	HR	16.8	1.67	15.2	2.3	
	BCOR 109	Talcschist	HR	25.8	−4.3			
	BCOR 110	Talcschist	HR	25.2	−5.4			
	BCOR 249-1	Talcschist	HR	21.4	−5.91	16.2	-5.6	
	BCOR 249-2	Talcschist	HR	23.1	−5.19			
TRIASSIC Meta-evaporites Rauhwacke	BCOR 250b-1	Cataclasite	HR	25.3	−1.2			
	BCOR 250b-2	Cataclasite	HR	25	−0.2			
	BCOR 250c-1	Cataclasite	HR	23.4	−1.7			
	BCOR 250c-2	Cataclasite	HR	23.5	−0.5			
	BCOR 250e	Cataclasite	HR	16.2	−2	18.4	−1.8	
JURASSIC Dolomitic marbles	BCOR 25	Dolomitic marble	HR			19.7	1.8	0.708306 ± 9
			Vein			19.8	2	0.708319 ± 15
	BCOR 27	Dolomitic marble	HR			21.8	2.2	0.707863 ± 9
			Vein			19.1	2.2	0.708175 ± 12
	BCOR 28	Dolomitic marble	HR			21.8	2.4	
NEOCOMIAN Marls	BCOR 30	Pure marble	HR	21.8	2.1			0.707766 ± 14
	BCOR 31	Pure marble	HR	17.4	2.1			
	BCOR 32	Phyllite-rich marble	HR	19.5	2.1			
	BCOR 33	Pure marble	HR	18.3	2.1			0.707300 ± 11
			Vein	19.3	2.3			
	BCOR 34	Phyllite-rich marble	HR	18.5	2.4			
			Vein	18.4	2.2			
	BCOR 35	Phyllite-rich marble	HR	17.4	2.9			
UPPER APTIAN Pure marbles	BCOR 36	Pure marble	HR	15.9	2.7			
			Vein	16.2	1.6			
	BCOR 92a	Calcite	Vein	17.3	0.9			0.708312 ± 16
	BCOR 92b	Calcite	Vein	17.4	1			
	BCOR 96	Pure marble	HR	17.3	2.9			0.707429 ± 12
			Vein	17.5	2.8			
	BCOR 97	Pure marble	Vein	14.8	3.6			
	BCOR 98	Pure marble	HR	15.9	2.8			0.707492 ± 13
			Vein	15.3	2.8			
	BCOR 99	Pure marble	HR	19.1	3.6			0.707552 ± 11
			Vein	19.6	2.6			
	BCOR 100	Pure marble	HR	13.6	3			0.707815 ± 13
			Vein	13.5	2.2			
	BCOR 101	Pure marble	HR	11.6	2.4			
			Vein	12.4	1.7			

deposit, further east in the NPZ. The fact that equilibrium between veins and host rocks is maintained along the section (Fig. 13b) is consistent with the fact that fluids circulated during deformation, with the ductile deformation allowing the isotopic equilibrium between pervasively deformed host marbles and the invading fluids (Urai 1983; Etheridge et al. 1983; Géraud et al. 1995; Sibson and Rowland 2003; Violay et al. 2015).

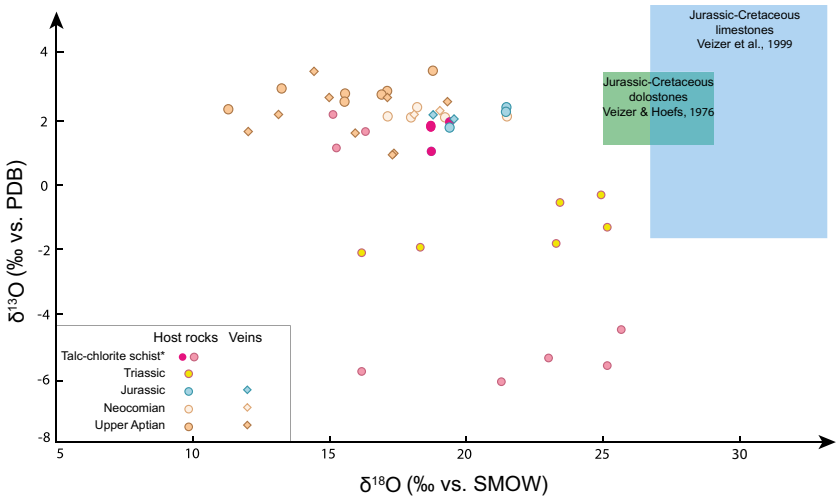

Fig. 11 C and O isotope compositions of carbonates from the Saraillé massif. Reported is also the field of Jurassic-Cretaceous marine limestones (blue) (Veizer et al. 1999) and Jurassic-Cretaceous marine dolostones (green) (Veizer and Hoefs 1976). The circles represent isotope compositions of host rocks and the diamonds represent isotope compositions of veins. * corresponds to pink-coloured talc schist for pink-pronounced circles and to graduated talcificated rocks for light pink circles

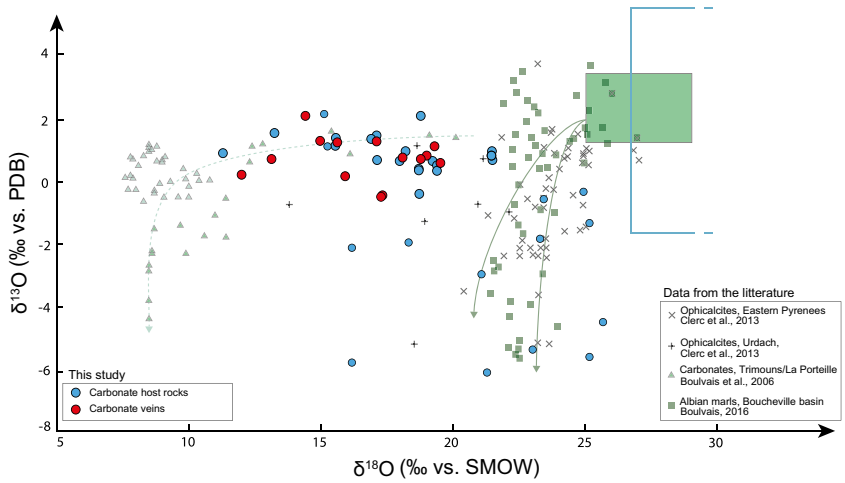

Fig. 12 C and O isotopes compositions of carbonates from the Saraillé massif compared to isotope composition from literature (Ophicalcites from Eastern Pyrenees (Clerc et al. 2013); Ophicalcites from Urdach massif ('Chaînons Béarnais') (Clerc et al. 2013); Carbonates from La Porteille/Trimouns (Boulvais et al. 2006) and Albian marls from Boucheville basin (Boulvais 2016). Reported is also the field of Jurassic-Cretaceous marine limestones (blue) (Veizer et al. 1999) and Jurassic-Cretaceous marine dolostones (green) (Veizer and Hoefs 1976). The arrows represent the metasomatic trends for the Trimouns/La Porteille system (Boulvais et al. 2006) and the closed system evolution of the Boucheville Basin (Boulvais 2016)

In Fig. 14, we propose a model for fluid circulations during the detachment fault activity accompanying mantle rocks uplift. During the final stages of mantle exhumation, the peridotites reached shallow crustal levels and were serpentinized by Fluid 1 in Fig. 14. This fluid, originally seawater subsequently enriched in chemical elements leached from the serpentinized mantle rocks, interacted with various lithologies involved in the deformation along the detachment. This triggered the talc and Cr-rich clinochlore crystallization between the Jurassic dolomitic marbles and the mantle rocks in a portion of the detachment fault that recorded the complete disappearance of both the entire Variscan crust and its Permian–Triassic cover. In the upper crustal levels, this syn-kinematic metasomatism took place under a relatively hot thermal climate (between 150 and 250 °C considering chlorite thermometry (Fig. 8), temperatures up to 350 °C are proposed by Fortané et al. (1986), Clerc et al. (2015) and Corre et al. (2016).

A saline fluid (Fluid 2 in Fig. 14), circulated within the Mesozoic metasedimentary pile and likely originated through the interaction of Fluid 1 with the Triassic evaporitic levels. The fluid migration towards the top of the sedimentary pile may have been stopped against the Albian "Flysch Noir" impermeable layer, leading to fluid accumulation at the top of the Aptian marbles. This likely resulted in an increase in the fluid/rock ratio. The relations between the S0/S1 foliation and veining indicate that Fluid 2 migration occurred during ductile deformation of the metasedimentary

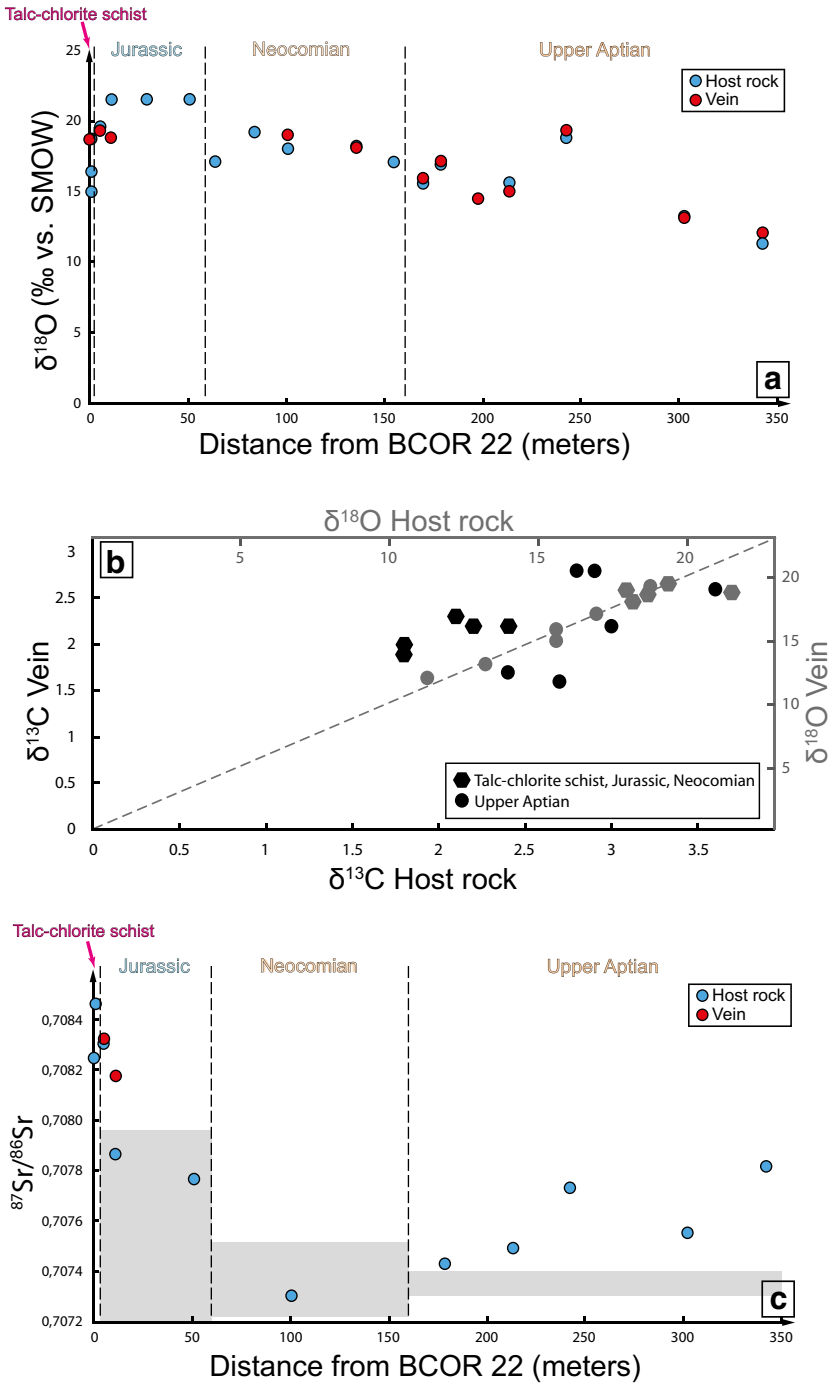

Fig. 13 C, O and Sr isotope compositions of carbonates from the Saraillé massif. **a** Evolution $\delta^{18}O$ value of the Mesozoic sedimentary cover from the talc-chlorite schist (BCOR 22) to the top. **b** Comparison between oxygen isotope compositions of veins and host rocks (grey) and comparison between carbon isotope compositions of veins and host rocks (black). **c** $^{87}Sr/^{86}Sr$ ratio of the Mesozoic sedimentary cover from the talc-chlorite schist (BCOR 22) to the top. Reported is also the field of Jurassic-Cretaceous marine limestones (grey) (Veizer et al. 1999)

pile, as suggested by the boudinage of some veins parallel to the flattening (Fig. 7g).

We may assume that the Albian "Flysch Noir" then underwent an in-situ decarbonation-dehydration process as described in equivalent formations in the Eastern Pyrenees (Boulvais 2016). This closed system evolution liberated another fluid that migrated upwards (Fluid 3, in Fig. 14), and is not characterized in the present study.

All these fluids circulated in a dynamic geological system where the pre-rift sedimentary cover was ductilely deformed during extreme crustal thinning and mantle exhumation. Duration of the metasomatic system was as long as the period of lithosphere extension, which lasted more than 10 Myr during the Albian-Cenomanian times.

Physical–chemical characteristics of the syn-kinematic fluids

Our fluid inclusion study in the Saraillé massif cover has revealed the presence of aqueous fluids with variable salinity.

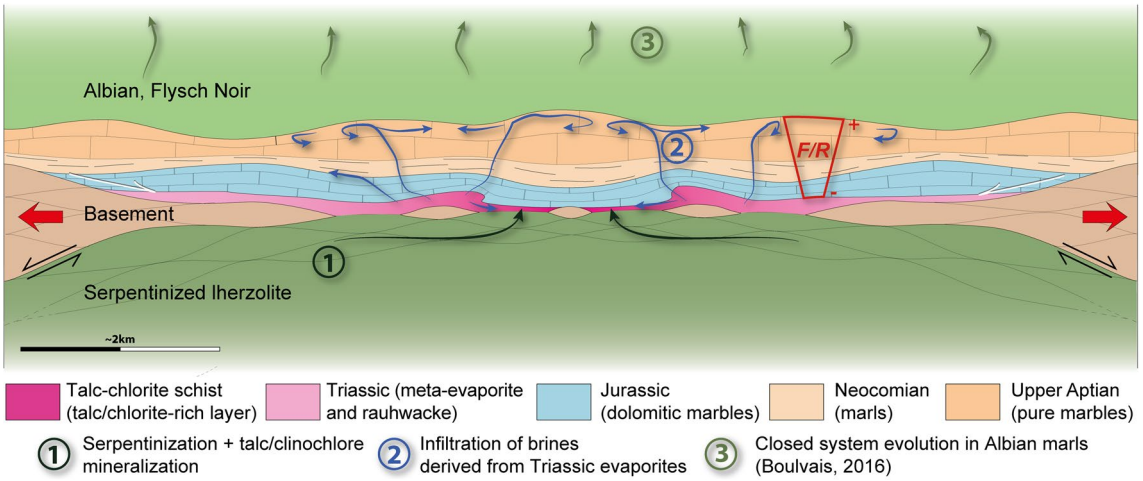

Fig. 14 Conceptual cross-section model based on field observations in the Saraillé massif showing the Albo-Cenomanian situation of the distal, hot passive margin with mantle exhumation (Corre et al. 2016) and the associated fluid events. (1) Serpentinization + talc/clinochlore mineralization, (2) Infiltration of brines derived from Triassic evaporites, (3) Closed system evolution in Albian marls

The carbonate (± quartz) vein network is characterized by two to three-phase fluid inclusions (liquid, gas, ± halite cube) witnessing salinity values ranging between 13 wt% and 34 wt% for fluids circulating through the Mesozoic cover. The Keuper evaporitic sediments on which the talc-chlorite schists pass laterally likely provided the saline elements. Where complete in the Pyrenean realm, the Keuper sedimentary succession consists of red, grey, and black shales, marls and evaporites (see in section II.2 above) (Salvany 1990; Flinch and Casas 1996; Calvet et al. 2004; Saura et al. 2015). Evaporites consist in gypsum, halite and anhydrite that crystallized in association with diagenetic double terminated quartz (Tarr 1929; Frechengues et al. 1992). In the Sarrance anticline, the Triassic metasediments do not contain evaporites anymore but they include double terminated quartz (Fig. 7e), here interpreted as the insoluble relics of evaporites that otherwise have dissolved completely. We propose that the brines found in the studied fluid inclusions are the witnesses of the dissolved Triassic evaporites from the Sarrance anticline. The halogen signature of fluid inclusions (Cl/Br for example) would have helped to confirm this proposal, but considering the quality and size of the fluid inclusions, this type of analysis was not possible. The complete transformation of the Triassic beds occurred in the talc-chlorite rich layer. As proposed above, this metasomatic layer partly resulted from the circulation of fluid evolved from the serpentinization of the mantle rocks. It gradually passes to the Triassic sequence exposed in the core of the Sarrance anticline and represents the final stages of fluid/rock interactions along a detachment that preserved only strongly thinned post-Triassic layers.

Some fluid inclusions exhibit specific gas-content depending on their stratigraphic position, like CH_4 (10%) and N_2 (90%) near the base of the pile and H_2S near the top (Table 5). Variable interaction of fluids with surrounding rocks, as suggested by Sr isotopes, may lead to variable contents of dissolved gas species (CH_4, H_2S, N_2) in the aqueous fluids.

Comparison with fluid circulations described in the NPZ

Salardon et al. (2017) have undertaken a study of the interactions between tectonics and fluid circulations in the Mesozoic carbonate rocks of the entire 'Chaînons Béarnais' range. They propose that the Cretaceous hyper-extension was coeval with cements precipitated from ascending magmatic alkaline fluids with high salinities, temperatures around 300 °C, and H_2S due to Thermo-Sulfato-Reduction (TSR) in Triassic evaporites. These fluids are rather similar (salinity, presence of $N_2 + CH_4$, H_2S) to the fluids evidenced in the Saraillé system, for which, moreover, interaction with mantle rocks is documented by the high Cr content of chlorite.

A major occurrence of brines reported from metasomatic rocks of the NPZ is located in the Trimouns/La Porteille system (Saint Barthélémy massif) (Boiron et al. 2007) (Eastern NPZ, Fig. 1). The Trimouns/La Porteille system is a world famous talc-chlorite deposit (Fortuné 1971; Moine et al. 1989) located in a detachment zone between the gneissic dome of the Saint Barthélémy massif and a thrusted unit composed of Paleozoic marbles, dolomites and black shales (Boulvais et al. 2006; Boiron et al. 2007). A hydrothermal activity responsible for the talc neo-formation has been dated between 112 and 97 Ma (Schärer et al. 1999) synchronous to the ZNP basins opening, even if the metasomatic history, notably chloritization, may have started during the lower Jurassic (Boutin et al. 2015) in relation to rifting at that time. Boiron et al. (2007) and Leisen et al. (2012) proposed that the talc deposit of Trimouns/La Porteille formed

through the infiltration of brines originated from seawater evaporation that further interacted with dolomitic units. In the Fig. 15, we compared the O and C isotope trends of the carbonates from the Trimouns/La Porteille and the Saraillé metasomatic systems. Actually, the trend calculated at Trimouns/La Porteille (Boulvais et al. 2006) was simply copied and pasted on the Saraillé data (at a somewhat higher $\delta^{13}C$ level); alteration of carbonates in the Saraillé massif follows the Trimouns/La Porteille trend even if, for the former, alteration did not give rise to talc mineralization (we recall here that the talc-chlorite schists at the base of the Saraillé succession formed by upward migration of aqueous fluids that have interacted with mantle rocks; Fig. 14). In the Trimouns/La Porteille system, there is a lack of a mantle component; it should be noted however that mantle rocks are known in the southern part of the St Barthélémy Massif (De Saint Blanquat et al. 2016). Our study in the Saraillé Massif, where we document brine production by dissolution of evaporites sheds some light on the understanding of the Trimouns/la Porteille world-class deposit, where massive brines circulation is documented.

DeFelipe et al. (2017) have undertaken a study of stable and clumped isotope analysis in carbonates of the westernmost outcrop of peridotites in the Pyrenean-Cantabrian belt located in Ziga (eastern Basque-Cantabrian basin). They compare their results with the ophicalcite occurrences of the Urdach massif and Lherz massif, in the North-Pyrenean Zone. They propose that the peridotite-hosted calcite veins yielded three different results: (i) from cold meteoric fluids affecting a primary carbonate phase (typical ophicalcites, Ziga); (ii) from a later recrystallization in a hot and saline environment (200–230 °C, Urdach); and (iii) from meteoric fluids at relatively low temperature (32–42 °C, Lherz). They suggest that hot and saline fluids result from the interaction with the detachment layer of the Keuper evaporites and with the mantle rocks and circulating through the Upper Cretaceous sediments. Thus, several aspects of the present system appear similar to the system in the Saraillé massif.

The partial dolomitization processes described in the Saraillé massif metasomatic system can also be compared to similar processes in the system of the Ason valley, located in the Basque Cantabrian basin (Northern Spain) (Lopez-Horgue et al. 2010). In this system, the dolomitization of Albian carbonates is related to a trans-tensional fault activity during Albian to Turonian times that involved a Triassic component. Hydrothermal fluids derived from evaporites at depth were channelized and heated along basement faults due to high geothermal gradients related to continental thinning processes. These fluids have recorded a temperature range between 75 °C and 240 °C and salinities of up to 22 wt% NaCl, also comparable to the system in the Saraillé massif.

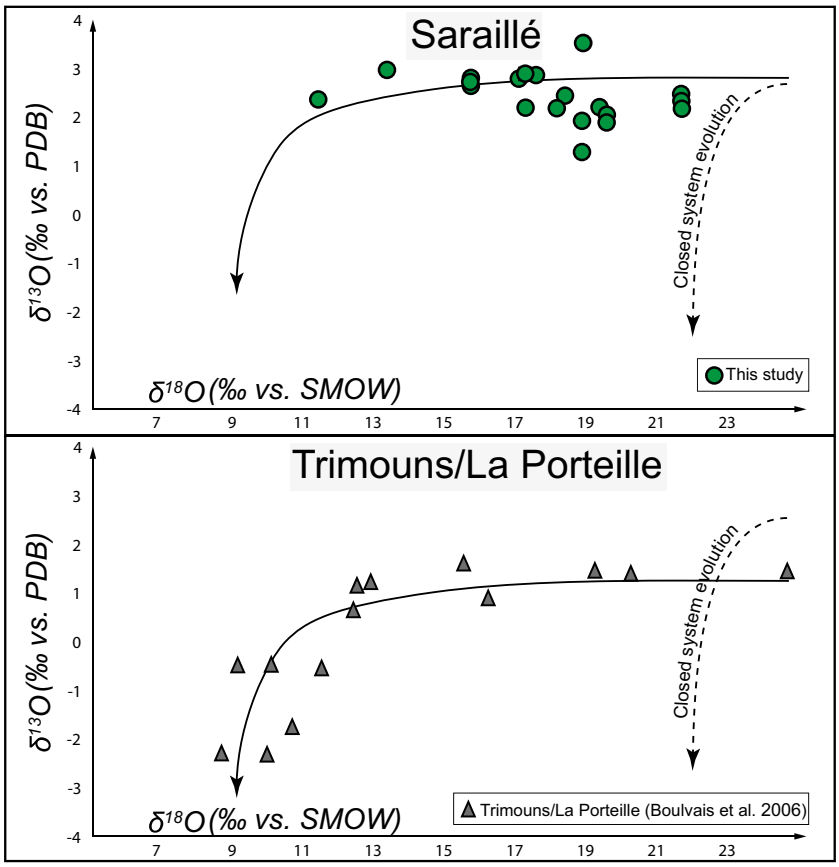

Fig. 15 Comparison between C and O isotope composition of the Saraillé massif and the Trimouns/La Porteille system (Boulvais et al. 2006). The closed system evolution corresponds to the Boucheville basin isotopes composition of Albian marls (Boulvais 2016)

Conclusions

In the Saraillé massif (Chaînons Béarnais, Pyrenees) fluids circulations occurred syn-kynematiccally in relation with the exhumation of subcontinental mantle rocks that took place in Mid-Cretaceous times. These circulations are recorded by (i) the presence of a talc-chlorite schists metasomatic layer in the detachment fault that exhumed the serpentinized lherzolites, (ii) the presence of a dense network of carbonated veins in the ductilely deformed carbonates of the detached pre-rift cover, (iii) the oxygen isotope alteration of this pre-rift Mesozoic cover. Fluids evolved from the serpentinized mantle as documented by the enrichment in Cr of newly formed chlorite; interaction with the Triassic evaporites levels is witnessed by the variable and high salinities (up to 34 wt% Eq. NaCl) recorded in some fluid inclusions. We propose a global model of fluid circulation in which a fluid, enriched in chemical elements leached from the serpentinized mantle rocks interacted with various lithologies involved along the detachment between the mantle rocks and the pre-rift Mesozoic sedimentary cover. This triggered the talc and Cr-rich clinochlore mineralization under relatively hot thermal conditions. A second fluid, displaying high salinity values (up to 34 wt% NaCl) was generated by the interaction with the Triassic metasediments and circulated within the overlying sediments resulting in an intense calcite vein network. The relations between the S0/S1 foliation and veining indicate that this circulation occurred during the extensional Pyrenean phase at Albian-Cenomanian times. Complete transformation of the Triassic beds occurred in the talc-chlorite rich layer that marks the detachment fault between the mantle rocks and the pre-rift Mesozoic sedimentary cover. We also propose that the upward migration of saline fluids was limited upward because of the presence of impermeable Albian "Flysch Noir" at the top of the pre-rift metasedimentary pile. The interplay between mantle exhumation, ductile deformation and fluid circulation proposed for the Saraillé massif sheds light on to the other metasomatic systems documented elsewhere in the Pyrenees, notably the Trimouns/La Porteille world famous talc deposit. It may also represent a reference for analogue active systems of limited access that developed during the formation of some present-day passive margins where extreme crustal thinning and mantle exhumation was accompanied by intense fluid circulation.

Acknowledgements This work was made possible through a grant from a PhD thesis (Corre B.), RGF project (Référentiel Géologique de la France) of the "Bureau de Recherches Géologiques et Minières" (BRGM, Thierry Baudin, manager) and a Master 2 (Marasi L.), ANR Pyramid (Mary Ford, manager). We are thankful to the two anonymous reviewers and to the journal editor Maarten A.T.M. Broekmans for their reviews and comments that helped to improve the quality of the manuscript. Riccardo Asti corrected the English.

References

Alonso-Zarza AM (2003) Palaeoenvironmental significance of palustrine carbo-nates and calcretes in the geological record. Earth Sci Rev 60:261–298

Biteau JJ, Le Marrec A, Le Vot M, Masset JM (2006) The aquitaine basin. Pet Geosci 12(3):247–273

Boiron MC, Cathelineau M, Dubessy J, Fabre C, Boulvais P, Banks D (2007) Fluid inclusion chemistry and stable isotope evidence for the circulation of brines at the basement-cover interface: the formation of the Trimouns Talc deposit. Proceedings of the ECROFI XIX conference, Bern, July 2007

Bonatti E, Seyler M, Channell J, Giraudeau J, Mascle G (1990) Peridotites drilled from the Tyrrhenian sea, ODP LEG 107. Proc Ocean Drill Program Sci Results 107:37–47

Boulvais P (2016) Fluid generation in the Boucheville Basin as a consequence of the North Pyrenean Metamorphism. CR Geosci 348(3):301–311

Boulvais P, De Parseval P, D'Hulst A, Paris P (2006) Carbonate alteration associated with talc-chlorite mineralization in the eastern Pyrenees, with emphasis on the St. Barthelemy Massif. Mineral Petrol 88(3–4):499–526

Boulvais P, Ruffet G, Cornichet J, Mermet M (2007) Cretaceous albitization and dequartzification of Hercynian peraluminous granite in the Salvezines Massif (French Pyrénées). Lithos 93(1):89–106

Bourdelle F, Cathelineau M (2015) Low-temperature chlorite geothermometry: a graphical representation based on a T–R2+–Si diagram. Eur J Mineral 27(5):617–626

Boutin A, de Saint Blanquat M, Poujol M, Boulvais P, de Parseval P, Rouleau C, Robert JF (2015) Succession of Permian and Mesozoic metasomatic events in the eastern Pyrenees with emphasis on the Trimouns talc-chlorite deposit. Int J Earth Sci 105(3):747–770

Calvet F, Anglada E, Salvany JM (2004) El Triasico de los Pirineos. Geol Esp 272–274

Canérot J, Hudec MR, Rockenbauch K (2005) Mesozoic diapirism in the Pyrenean orogen: salt tectonics on a transform plate boundary. Am Assoc Pet Geol Bull 89(2):211–229

Castéras (1970) Oloron Sainte-Marie, geological map of France, 1/50 000, n° 1051. Bureau de Recherche Géologique et Minière, Orléans

Choukroune P (1989) The ECORS Pyrenean deep seismic profile reflection data and the overall structure of an orogenic belt. Tectonics 8:23–39

Choukroune P (1992) Tectonic evolution of the Pyrenees. Annu Rev Earth Planet Sci 20:143–158

Choukroune P, Mattauer M (1978) Tectonique des plaques et Pyrénées; sur le fonctionnement de la faille transformante nord-pyrénéenne; comparaisons avec des modèles actuels. Bull Soc Géol Fr 7(5):689–700

Clerc C, Lagabrielle Y (2014) Thermal control on the modes of crustal thinning leading to mantle exhumation: insights from the Cretaceous Pyrenean hot paleomargins. Tectonics 33(7):1340–1359

Clerc C, Boulvais P, Lagabrielle Y, de Saint Blanquat M (2013) Ophicalcites from the northern Pyrenean Belt: a field, petrographic and stable isotope study. Int J Earth Sci 1–23

Clerc C, Lahfid A, Monié P, Lagabrielle Y, Chopin C, Poujol M, Boulvais P, Ringenbach JC, Masini E, De St Blanquat M (2015) High-temperature metamorphism during extreme thinning of the continental crust: a reappraisal of the north Pyrenean passive paleomargin. Solid Earth 6:643–668

Corre B, Lagabrielle Y, Labaume P, Fourcade S, Clerc C, Ballèvre M (2016) Deformation associated with mantle exhumation in a distal, hot passive margin environment: new constraints from the Saraillé Massif (Chaînons, North-Pyrenean Zone). Compt Rendus Géosci 348(3–4):279–289

Dauteuil O, Ricou LE (1989) Hot-fluid circulation as an origin for the North Pyrenean cretaceous metamorphism. Geodin Acta 3(3):237–250

De Saint Blanquat M, Bajolet F, Grand'Homme A, Projetti A, Zanti M, Boutin A, Clerc C, Lagabrielle Y, Labaume P (2016) Cretaceous mantle exhumation in the central Pyrenees: new constraints from the peridotites in eastern Ariège (North Pyrenean zone, France). Compt Rendus Géosci 348(3–4):279–289

Debroas EJ (1990) Le flysch noir albo-cenomanien témoin de la structuration albienne à sénonienne de la Zone nord-pyrénéenne en Bigorre (Haute-Pyrénées, France). Bull Soc Géol Fr 8(2):273–285

DeFelipe I, Pedreira D, Pulgar JA, Iriarte E, Mendia M (2017) Mantle exhumation and metamorphism in the Basque-Cantabrian Basin (N Spain): stable and clumped isotope analysis in carbonates and comparison with ophicalcites in the North-Pyrenean Zone (Urdach and Lherz). Geochem Geophys Geosyst 18(2):631–652

Dubessy J, Poty B, Ramboz C (1989) Advances in C-O-H-N-S fluid geochemistry based on micro-Raman spectrometric analysis of fluid inclusions. Eur J Mineral 1(4):517–534

Etheridge MA, Wall VJ, Vernon RH (1983) The role of the fluid phase during regional metamorphism and deformation. J Metamorph Geol 1(3):205–226

Fallourd S, Poujol M, Boulvais P, Paquette JL, de Saint Blanquat M, Rémy P (2014) In situ LA-ICP-MS U–Pb titanite dating of Na–Ca metasomatism in orogenic belts: the North Pyrenean example. Int J Earth Sci 103(3):667–682

Flinch JF, Casas JM (1996) Inversion of a transfer system into lateral ramps: an example from the South-Central Pyrenees (Spain). Geol Rundsch 85:372–379

Fortané A, Duée G, Lagabrielle Y, Coutelle A (1986) Lherzolites and the western « Chaînons Béarnais » (French Pyrenees): structural and paleogeographical pattern. Tectonophysics 129:81–98

Fortuné JP (1971) Contribution à l'étude minéralogique et génétique des talcs pyrénées. PhD thesis, Université Paul Sabatier, Toulouse, p 237

Frechengues M, Peybernes B, Lucas CL, Souquet P (1992) Le Trias des Pyrénées centrales et orientales Franco-Espagnoles. Actes du Laboratoire de Geologie sédimentaire et paléontologique de l'Université. Paul Sabatier Toulouse STRATA 17(2):90

Früh-Green GL, Connolly JAD, Plas A (2004) Serpentinization of oceanic peridotites: implications for geochemical cycles and biological activity. Geophys Monogr Ser 144:119–136

Géraud Y, Caron JM, Faure P (1995) Porosity network of a ductile shear zone. J Struct Geol 17(12):1757–1769

Golberg JM, Leyreloup AF (1990) High temperature-low pressure Cretaceous metamorphism related to crustal thinning (Eastern North Pyrenean Zone, France). Contrib Mineral Petrol 104:194–207

Gong Z, Van Hinsbergen DJJ, Dekkers MJ (2009) Diachronous pervasive remagnetization in northern Iberian basins during Cretaceous rotation and extension. Earth Planet Sci Lett 284(3):292–301

Incerpi N, Martire L, Manatschal G, Bernasconi SM (2017) Evidence of hydrothermal fluid flow in a hyperextended rifted margin: the case study of the Err nappe (Se Switzerland). Swiss J Geosci 110(2):439–456

Jammes S, Manatschal G, Lavier L, Masini E (2009) Tectonosedimentary evolution related to extreme crustal thinning ahead of a propagating ocean: example of the western Pyrenees. Tectonics 28(4):TC4012. https://doi.org/10.1029/2008TC002406

Jammes S, Lavier L, Manatschal G (2010) Extreme crustal thinning in the Bay of Biscay and the Western Pyrenees: from observations to modeling. Geochem Geophys Geosyst 11(10):Q10016. https://doi.org/10.1029/2010GC003218

Lagabrielle Y, Bodinier JL (2008) Submarine reworking of exhumed subcontinental mantle rocks: field evidence from the Lherz peridotites, French Pyrenees. Terra Nova 20(1):11–21

Lagabrielle Y, Labaume P, de Saint Blanquat M (2010) Mantle exhumation, crustal denudation, and gravity tectonics during Cretaceous rifting in the Pyrenean realm (SW Europe): insights from the geological setting of the lherzolite bodies. Tectonics 29(4):TC4012. https://doi.org/10.1029/2009TC002588

Lanaja JM, Querol R, Navarro A (1987) Contribucion de la Exploracion Petrolifera al Conocimiento de la Geologia de Espana, Instituto Geologicó y Minero de España, IGME:pp 1–46

Leisen M, Boiron MC, Richard A, Dubessy J (2012) Determination of Cl and Br concentrations in individual fluid inclusions by combining microthermometry and LA-ICPMS analysis: implications for the origin of salinity in crustal fluids. Chem Geol 330/331:197–206

Lopez-Horgue MA, Iriarte E, Schröder S, Fernandez-Mendiola PA, Caline B, Corneyllie H, Frémont J, Sudrie M, Zertie S (2010) Structurally controlled hydrothermal dolomites in Albian carbonates of the Ason valley, Basque Cantabrian Basin, Northern Spain. Mar Pet Geol 27:1069–1092

Machel HG (2001) Bacterial and thermochemical sulfate reduction in diagenetic settings–old and new insights. Sediment Geol 140:143–175

Manatschal G (2004) New models for evolution of magma-poor rifted margins based on a review of data and concepts from West Iberia and Alps. Int J Earth Sci 93:432–466

Manatschal G, Müntener O (2009) A type sequence across an ancient magma-poor ocean-continent transition: the example of the western Alpine Tethys ophiolites. Tectonophysics 473:4–19

Manatschal G, Nievergelt P (1997) A continent-ocean transition recorded in the Err and Platta nappes (eastern Switzerland). Eclogae Geol Helv 90:3–27

McCrea JM (1950) On the isotopic chemistry of carbonates and a paleotemperature scale. J Chem Phys 18(6):849–857

Moine B, Fortune JP, Moreau P, Viguier F (1989) Comparative mineralogy, geochemistry, and conditions of formation of two metasomatic talc and chlorite deposits; Trimouns (Pyrenees, France) and Rabenwald (Eastern Alps, Austria). Econ Geol 84(5):1398–1416

Mouthereau F, Filleaudeau PY, Vacherat A, Pik R, Lacombe O, Fellin MG, Masini E (2014) Placing limits to shortening evolution in the Pyrenees: role of margin architecture and implications for the Iberia/Europe convergence. Tectonics 33(12):2283–2314

Muñoz JA (1992) Evolution of a continental collision belt: ECORS-Pyrenees crustal balanced cross-section. Thrust Tectonics. Springer Netherlands:235–246

Olivet JL (1996) La cinématique de la plaque ibérique. Bull Cent Rech Explor Prod Elf Aquitaine 20(1):131–195

Péron-Pinvidic G, Manatschal G (2009) The final rifting evolution at deep magma-poor passive margins from Iberia-Newfoundland: a new point of view. Int J Earth Sci 98(7):1581–1597

Pinto VHG, Manatschal G, Karpoff AM, Viana A (2015) Tracing mantle-reacted fluids in magma-poor rifted margins: the example of Alpine Tethyan rifted margins. Geochem Geophys Geosyst 16(9):3271–3308

Pouchou JL, Pichoir F (1984) Un nouveau modèle de calcul pour la microanalyse quantitative par spectrometrie de rayons X – Partie I: application à l'analyse d'échantillons homogènes. La Recherche Aerospatiale (3):167–192

Poujol M, Boulvais P, Kosler J (2010) Regional-scale Cretaceous albitization in the Pyrenees: evidence from in situ U–Th–Pb dating of monazite, titanite and zircon. J Geol Soc 167(4):751–767

Reynolds SJ, Lister GS (1987) Structural aspects of fluid-rock interactions in detachment zones. Geology 15(4):362–366

Robertson AHF (2007) Evidence of continental breakup from the Newfoundland rifted margin (Ocean Drilling Program Leg 210): lower Cretaceous seafloor formed by exhumation of subcontinental mantle lithosphere and the transition to seafloor spreading. In Tucholke BE, Sibuet JC, Klaus A (Eds.), Proceedings of the

Ocean Drilling Program, Scientific results, 210: College Station, TX (Ocean Drilling Program):1–69

Roca E, Munoz JA, Ferrer O, Ellouz N (2011) The role of the Bay of Biscay Mesozoic extensional structure in the configuration of the Pyrenean orogen: constraints from the MARCONI deep seismic reflection survey. Tectonics 30(2):TC2001. https://doi.org/10.1029/2010TC002735

Roure F, Choukroune P, Berastegui X, Munoz JA, Villien A, Matheron P, Deramond J (1989) ECORS deep seismic data and balanced cross sections: geometric constraints on the evolution of the Pyrenees. Tectonics 8(1):41–50

Roux JC (1983) Recherches stratigraphiques et sédimentologiques sur les flysch crétacés pyrénéens au Sud d'Oloron (Pyrénées Atlantiques). Thèse 3ème cycles Université Paul Sabatier Toulouse

Salardon R, Carpentier C, Bellahsen N, Pironon J, France-Lanord C (2017) Interactions between tectonics and fluid circulations in an inverted hyper-extended basin: example of Mesozoic carbonate rocks of the western North Pyrenean Zone (Chaînons Béarnais, France). Mar Pet Geol 80:563–586

Salvany JM (1990) Introducción a las evaporiticas triasicas de las cadenas perifericas de la cuenca del Ebro: Catalánides, Pirineo y Región Cantábrica. In: Orit F, Salvany JM (eds) Formaciones evaporiticas de la Cuenca del Ebro y cadenas Perifericas, y de la zona de Levante. ENRESA-Universidade, Barcelone/ES, pp 9–20

Saura E, Ardevol i Oro L, Teixell A, Verges J (2015) Rising and falling diapirs, shifting depocenters, and flap overturning in the Cretaceous Sopeira and Sant Gervas subbasins (Ribagorça Basin, southern Pyrenees). Tectonics 35(3):638–662

Schärer U, de Parseval P, Polvé M, de Saint Blanquat M (1999) Formation of the Trimouns talc-chlorite deposit (Pyrenees) from persistent hydrothermal activity between 112 and 97 Ma. Terra Nova 11(1):30–37

Sibson R, Rowland JV (2003) Stress, fluid pressure and structural permeability in seismogenic crust, North Island, New Zealand. Geophys J Int 154:584–594

Sibuet JC, Srivastava SP, Spakman W (2004) Pyrenean orogeny and plate kinematics. J Geophys Res Solid Earth 109(B8):B08104. https://doi.org/10.1029/2003JB002514

Souquet P, Debroas JE, Boirie JM, Pons P, Fixari G, Roux JC, Dol J, Thieuloy JP, Bonnemaison M, Manivit H, Peybernes B (1985) The black flysch (Albian-early cenomanian) from the Pyrenees. Bull Centres Rech Explor Prod Elf-Aquitaine 9(1):183–252

Tarr WA (1929) Doubly terminated quartz crystals occurring in gypsum. Am Miner:19–25

Teixell A, Labaume P, Lagabrielle Y (2016) The crustal evolution of the west-central Pyrenees revisited: inferences from a new kinematic scenario. Compt Rendus Géosci 348(3–4):257–267

Urai JL (1983) Water assisted dynamic recrystallization and weakening in polycrystalline bischofite. Tectonophysics 96(1–2):125–157

Vacherat A, Mouthereau F, Pik R, Bellahsen N, Gautheron C, Bernet M, Daudet M, Balansa J, Bouchaib T, Rosella Pinna J, Radal J (2016) Rift-to-collision transition recorded by tectonothermal evolution of the northern Pyrenees. Tectonics 35(4):907–933

Vauchez A, Clerc C, Bestani L, Lagabrielle Y, Chauvet A, Lahfid A, Mainprice D (2013) Preorogenic exhumation of the North Pyrenean Agly massif (Eastern Pyrenees-France). Tectonics 32(2):95–106

Veizer J, Hoefs J (1976) The nature of O18/O16 and C13/C12 secular trends in sedimentary carbonate rocks. Geochim Cosmochim Acta 40(11):1387–1395

Veizer J, Ala D, Azmy K, Bruckschen P, Buhl D, Bruhn F, Jasper T (1999) 87Sr/86Sr, δ13C and δ18O evolution of Phanerozoic seawater. Chem Geol 161(1):59–88

Vergés J, Fernàndez M, Martínez A (2002) The Pyrenean orogen: pre-, syn-, and post-collisional evolution. J Virtual Explor 8:57–76

Violay M, Gibert B, Mainprice D, Burg JP (2015) Brittle versus ductile deformation as the main control of the deep fluid circulation in oceanic crust. Geophys Res Lett 42:2767–2773

Whitney DL, Evans BW (2010) Abbreviations for names of rock-forming minerals. Am Miner 95:185–187

Wiewióra A, Weiss Z (1990) Crystallochemical classifications of phyllosilicates based on the unified system of projection of chemical composition: II. The chlorite group. Clay Miner 25(1):83–92